Original paper

Review of zeolite mineralizations from the high-grade metamorphosed Strážek Unit, Moldanubian Zone, Czech Republic

Milan NOVÁK[1], Jiří TOMAN[2]*, Radek ŠKODA[1], Drahoš ŠIKOLA[3], Jiří MAZUCH[3]

[1] *Department of Geological Sciences, Faculty of Science, Masaryk University, Kotlářská 2, CZ-611 37 Brno, Czech Republic*
[2] *Department of Mineralogy and Petrography, Moravian Museum, Zelný trh 6, CZ-659 37 Brno, Czech Republic, email: jtoman@mzm.cz*
[3] *Diamo, S. E., Branch GEAM, CZ-592 51 Dolní Rožínka, Czech Republic*
** Corresponding author*

Geological position, mineral assemblages, and compositional evolution of several types of mostly hydrothermal zeolite mineralizations were examined in the easternmost part of the Moldanubian Zone (Strážek Unit), Czech Republic, using EPMA and Raman spectroscopy. The zeolite mineralizations are related to the following geological processes: (A1) late magmatic to (A2, A3) hydrothermal crystallization (pseudomorphs, brittle tectonic fractures) in granitic pegmatites; (B) retrograde stages of the Variscan metamorphism – (B1) Alpine-type hydrothermal veins on ductile to brittle fractures with epidote, prehnite and zeolites, (B2) laumontite and (B3) natrolite veinlets; the latter two on thin brittle fissures; (C) hydrothermal zeolite veins with dominant stilbite-(Ca) + heulandite-(Ca) and sulfides on ductile to brittle fractures, and (D) thin brittle fissure-filling veinlets lined with harmotome ± calcite. The zeolite mineralizations include pollucite (A), analcime (A, B), phillipsite-(Ca) (A), harmotome (A, D), chabazite-(Ca) and chabazite-(K) (A, B), thomsonite-(Ca) (A), natrolite (A, B), laumontite (A, B, C), stilbite-(Ca) (B, C), scolecite (B), and heulandite-(Ca) (B, C). The individual zeolite mineralizations differ significantly in their regional distribution: (B) Alpine-type hydrothermal veins and laumontite and natrolite veinlets are widespread within almost the whole region, whereas zeolites in (A) granitic pegmatites and in (C, D) hydrothermal veins are concentrated along the eastern border of the Strážek Unit, the latter two assemblages restricted to the Rožná-Olší ore field. Fluids with variable composition and origin facilitated the formation of individual zeolite mineralizations. They evolved from moderate-T (~400 °C) to low-T (~50 °C) conditions characterized by the following extra-framework cations ± volatiles with dominant H_2O: (A1) – Cs, Ba, Ca, Na > K, (A2) – Ca, K, Ba > Na, (A3) – Ca, Na, Ba (A: T ~400–50 °C); (B1) – Ca ± B, (B2) – Ca, (B3) – Na, Ca (B: T ~350–50 °C); (C) – Ca > Na ± S, F (C: T ~240–50 °C); (D) – Ba, Ca ± CO_2 (D: T ~100–50 °C). Sources of fluids include – residual fluids exsolved from pegmatite melt (A1) and external fluids derived from host rock (A2, A3); fluids related to retrograde stages of the Variscan metamorphism (A3?, B1, B2, B3, C?); likely post-Variscan fluids of various origin (C, D). The zeolite assemblages demonstrate that the PTX conditions suitable for their origin were attained in the late stages of distinctive geological processes. Zeolites may be used as a valuable indicator of alkaline to neutral and low-T to very low-T hydrothermal fluids with high activity of Ca, K, Na and/or Ba, and variable $a\mathrm{SiO_2}$ on tectonic fractures and fissures.

Keywords: zeolites, mineral assemblages, chemical composition, Strážek Unit, Moldanubian Zone
Received: 23 February 2022; accepted: 24 April 2023; handling editor: M. Števko
The online version of this article (doi: 10.3190/jgeosci.370) contains supplementary electronic material.

1. Introduction

Zeolite mineralizations originated in a wide spectrum of hydrothermal environments in magmatic, metamorphic and sedimentary rocks (e.g., Hay and Sheppard 2001; Langella et al. 2001; Utada 2001a; Ming and Boettinger 2001; Dill et al. 2007) and especially within volcanic rocks and volcano-sedimentary sequences (e.g., Stefansson and Gíslason 2001; Utada 2001b; Weisenberger and Selbekk 2009; Spürgin et al. 2019). They typically crystallized during the late low-T stages of the geological evolution of the host rock complexes. Zeolites typically formed during metamorphism of zeolite facies (e.g., Utada 2001a). Additionally, zeolites occur at Alpine-type hydrothermal veins facilitated by intensive tectonic fracturing and availability of H_2O-rich fluids, which manifest retrograde stage of regional metamorphism (e.g., Weisenberger 2009; Weisenberger and Bucher 2010, 2011) as well as in fracture network associated with major faults (e.g., San Andreas, California – James and Silver 1988; Gole Larghe Fault Zone, Southern Alps – Dempsey et al. 2014). Their mineral assemblages reflect chiefly the temperature and chemical composition of host rocks and of acting fluids; the host rock supplied most cations entering zeolite structures (Weisenberger and Bucher 2010, 2011). Zeolites also are common in peralkaline pegmatites (e.g., Schilling et al. 2011 and references therein) but quite rare in granitic pegmatites of both petrochemical families LCT (Li–Cs–Ta) and NYF (Nb–Y–F) where they commonly occur as the latest minerals in pockets along with clay

minerals and carbonates (London et al. 2012; Černý et al. 2012; Pieczka et al. 2015). Only exceptionally zeolites are associated with primary magmatic pollucite (Teertstra et al. 1995; Toman and Novák 2018). Zeolites, typically harmotome, were also found in hydrothermal veins at Pb,Zn,Ag-ore deposits (e.g., Sahama and Lehtinen 1967; Řídkošil and Knížek 1987; Litochleb et al. 2000; Green et al. 2005; Larsen et al. 2005; Pauliš et al. 2014), and in the Rožná U-deposit, Strážek Unit (Pauliš and Šikola 1999; Novák et al. 2001; Kříbek et al. 2009).

We studied zeolite mineralizations in various rocks from the Strážek Unit, the easternmost part of the Moldanubian Zone, to recognize their distinctive regional, geological, mineralogical, and compositional features. This pioneering study of zeolites in the Moldanubian Zone is a basis for a detailed examination of zeolite mineralization from U-deposits in the Rožná–Olší ore field and their relations to the processes producing U-mineralizations. We focused on (i) late magmatic to hydrothermal zeolites from the granitic pegmatites (Černý 1965a; Toman and Novák 2018), (ii) a variety of zeolite-bearing Alpine-type hydrothermal veins (Vávra 1997), and on (iii) zeolites from the hydrothermal veins associated with mineralized shear zones in the Rožná–Olší ore field situated along the eastern border of the Strážek Unit (Pauliš and Šikola 1999; Kříbek et al. 2009). We also discussed the tectonic character of fractures in the rocks hosting zeolites, PT conditions of their origin, and potential sources of hydrothermal fluids for the distinctive zeolite mineralizations.

2. Geological and mineralogical background

2.1. Regional geology

The Moldanubian Zone, the highly metamorphosed core of the Bohemian Massif, represents a crustal (and upper mantle) tectonic collage assembled during the Variscan orogeny (~370–300 Ma). It was modified by several events of superimposed deformations and high- to low-grade metamorphic recrystallizations and intruded by numerous Carboniferous *I*-type to *S*-type granitic plutons. Two main lithotectonic units with distinct lithologies were defined: (i) Drosendorf Unit, structurally divided on the lowermost Monotonous Group encompassing mainly migmatitic paragneisses intercalated with minor orthogneiss, quartzite, and amphibolite. It is overlain by the Varied Group, including paragneisses with abundant intercalations of amphibolite, calcite and dolomite marbles, quartzite, graphite schist, and calc-silicate rocks. Both groups are overlain by (ii) the structurally highest Gföhl Unit comprising felsic granulites, mostly strongly serpentinized peridotites, eclogites and migmatitic Gföhl orthogneisses (e.g., Matte et al. 1990; Finger et al. 1997; Guy et al. 2011; Schulmann et al. 2014). The eastern part of the Moldanubian Zone, the Strážek Unit, is built of the high-grade Gföhl Unit and Varied Group.

The metamorphic rocks underwent a polyphase metamorphic evolution; an HT-HP event in upper amphibolite to granulite facies at $T_{max.}$ ~850–900 °C and $P_{max.}$ = 1.2–1.8 GPa dated at ~345–340 Ma (Kotková 2007) was overprinted during a rapid decompression by an HT–MP event at T < ~700 °C and P ~0.4–0.6 GPa (e.g., Tajčmanová et al. 2006; Pertoldová et al. 2009, 2010 and references therein), and this stage locally produced partial melting of rocks. Along with bodies of melasyenites (e.g., Drahonín body) related to the Třebíč pluton (Leichmann et al. 2017; Janoušek et al. 2020) and tourmaline-bearing leucogranites (Jiang et al. 2003; Buriánek and Novák 2007; Buriánek et al. 2016), common rare-element granitic pegmatites (e.g., Věžná, Rožná, Drahonín, Dolní Bory, Dobrá Voda, Strážek), dated at 338–323 Ma; (Novák et al. 1998; Melleton et al. 2012) intruded various metamorphic rocks of the Strážek Unit at a shallow crust level of P < ~0.2–0.3 GPa (Ackermann et al. 2007; Novák et al. 2013).

Three superimposed regional metamorphic foliations define the structural pattern of the Strážek Unit: (i) early, steeply dipping foliation with regional ~NNE–SSW strike is reworked into (ii) flat-lying fabric occurring in the central part of the Strážek Unit and (iii) NNW–SSE- to NNE–SSW-striking foliation in rocks from the eastern part of the Strážek Unit. The latter is interpreted as a result of E–W compression at lower crustal levels (Tajčmanová et al. 2006; Verner et al. 2009). The subsequent exhumation to middle crustal levels was associated with kilometer-scale isoclinal folding. Longitudinal N–S to NNW–SSE-striking ductile shear zones (Rožná and Olší shear zones) dip WSW at an angle of 70–90° and strike parallel to the tectonic contact between the Strážek Unit (dominant Gföhl Unit) and the Svratka Crystalline Complex. The origin of the shear zones is compatible with SW–NE normal and N–S dextral kinematics (Kříbek and Hájek 2005). Superimposed, mostly normal zones of brittle deformation are associated with graphite- and phyllosilicate-rich coherent and incoherent cataclasites and fault breccias, several cm to ~15 m thick, typically developed within the Rožná–Olší ore field.

2.2. Overview of zeolite mineralizations in the region

Zeolites are rare to locally common in the examined region and were studied in several different geological environments. This subchapter provides a brief overview of zeolite mineralizations described to date in order to manifest the high variability of petrogenetic types of zeolites in the region and chiefly to show our current stage of knowledge.

The most detailed studies have been performed to date on zeolites from the granitic pegmatites Věžná I, Věžná II and Drahonín VI. They include several distinct paragenetic types from zeolites (pollucite, analcime, chabazite-(Ca), harmotome) that originated in late primary magmatic to the early hydrothermal stage of pegmatite evolution (Věžná I; Toman and Novák 2018) to a variety of late alteration products. The zeolites (analcime, thomsonite-(Ca), phillipsite-(Ca)-harmotome, chabazite-(Ca), natrolite) occur in pseudomorphs after primary minerals (pollucite, oligoclase, quartz, cordierite, tourmaline) or more commonly on tectonic fractures and fissures mostly at the Věžná II pegmatite (Černý 1960, 1965a, b; Teertstra et al. 1995; Pauliš and Cempírek 1998; Dosbaba and Novák 2012; Toman and Novák 2018, 2020; Gadas et al. 2020; Čopjaková et al. 2021).

Alpine-type hydrothermal veins were studied in detail only at the locality Mirošov (Černý 1955; Vávra 1997). They are characterized by the occurrence of crystals growing on walls of tectonic fractures (quartz, epidote, prehnite, axinite, adularia, albite and late zeolites – stilbite-(Ca), heulandite-(Ca), chabazite-(K)). Strong hydrothermal alteration of host amphibolites is typical (Vávra 1997).

A variety of zeolite mineralizations was found during mining and prospection at the Rožná–Olší ore field (e.g., Kruťa 1966; Šťáva 1981; Pauliš and Šikola 1999; Novák et al. 2001; Kříbek and Hájek 2005). They occur in several structurally distinct positions, particularly within the Rožná U-deposit, mostly spatially related to the shear zones (Uhlík and Řídkošil 1987; Pauliš and Šikola 1999). Zeolite-rich assemblage was found at the Jasan Mine, 16th level; large crystals, up to 3 cm in size, of stilbite-(Ca), heulandite-(Ca), and chabazite, associating with pyrite are developed on fractures of amphibolite (Šťáva 1981). Harmotome is the most abundant zeolite on thin tectonic fissures (Pauliš and Šikola 1999; Kříbek and Hájek 2005).

The published papers, except those from granitic pegmatites, are typically brief descriptive mineralogical reports with a low number or absence of analytical data; mostly, unit-cell dimensions and SE and BSE images of zeolites are presented. Moreover, petrographic descriptions of host rocks, including their hydrothermal alterations and mutual relations of the particular zeolites and associated minerals, are commonly absent.

2.3. P–T–X stability of zeolites

Geochemical and PT conditions suitable for the formation of zeolites were outlined in numerous studies (see, e.g., Chipera and Apps 2001; Neuhoff et al. 2004; Weisenberger 2009; Weisenberger and Bucher 2010; Weisenberger et al. 2014 and references therein). Aqueous silica activity ($a\mathrm{SiO_2}$), concentrations of extra-framework cations (Ca, Na, K, Ba, Sr, Mg), and pH (alkaline to neutral) are the most important fluid parameters along with temperature, whereas pressure plays a lesser role (Weisenberger 2009); most zeolites crystallized at low-P conditions < 100 MPa. Additional less important factors include X_{CO2} and $f\mathrm{O_2}$.

We focused chiefly on equilibria in the system Ca–Al–Si–O–H (Fig. 1) because Ca-rich zeolites are dominant in almost all examined mineral assemblages. Zeolites with dominant Na (analcime, natrolite) are rare and occur mainly in granitic pegmatite Věžná I (Dosbaba and Novák 2012; Toman and Novák 2018; Čopjaková et al. 2021). The following diagrams demonstrate the stability of the individual zeolites and some associated minerals. Laumontite is a *high-T* zeolite stable at T < ~310 °C and P = 100 MPa (Fig. 1a), followed by heulandite-(Ca), which crystallized at T < ~310 °C but only at high $a\mathrm{SiO_2}$ (Fig. 1b) otherwise T < ~250 °C is feasible. A *low-T* zeolite stilbite-(Ca) is stable at T < ~170 °C and at P = 100 MPa (Fig. 1a), whereas chabazite-(Ca), further typical *low-T* zeolite, is stable at similar T < ~170 °C but at low $a\mathrm{SiO_2}$ (Fig. 1b). Harmotome has no experimental or calculated data about its PTX stability except for its hydrothermal synthesis at T = 95 °C (Perrotta 1976). Its paragenetic position in crystallization sequences of zeolites among the latest (e.g., Moles and Nawaz 1996; Toman and Novák 2018) suggests a similar PTX-stability field or lower T (< ~100 °C) than chabazite-(Ca). The experimental and calculated PTX data for analcime yielded a very high stability field at T ~300 to ~50 °C (e.g., Neuhoff et al. 2004; Weisenberger et al. 2014), and a wide range of T was found in natural systems (e.g., Chipera and Apps 2001). In general, low-T limits of most zeolites are about 110 to 50 °C (e.g., Chipera and Apps 2001; Weisenberger and Selbekk 2009) or even less (Apps 1983), and some zeolites (e.g., chabazite, thomsonite, mordenite, clinoptilolite) formed at T <40–50 °C (e.g., Apps 1983; Iijima 2001; Karlsson 2001; Utada 2001a; Weisenberger and Selbekk 2009).

3. Samples and methods

3.1. Samples

We studied zeolites from almost all known localities in the Strážek Unit (ESM 1). Nearly all studied samples of zeolites were obtained from the collection of the Moravian Museum, Brno, due to scarcity of zeolites in the studied region in general (e.g., Burkart 1953; Kruťa 1966; Šťáva 1981; Pauliš and Šikola 1999), lack of outcrops in this morphologically flat area (except for the active quarry in Mirošov and several old quarries), as well as very limited access to the U-mines closed at 1994. The examined samples of zeolites were collected from 1924 to the early 1990^{ies} (ESM 1); hence, their geological background is mostly poor. Also, all samples from the

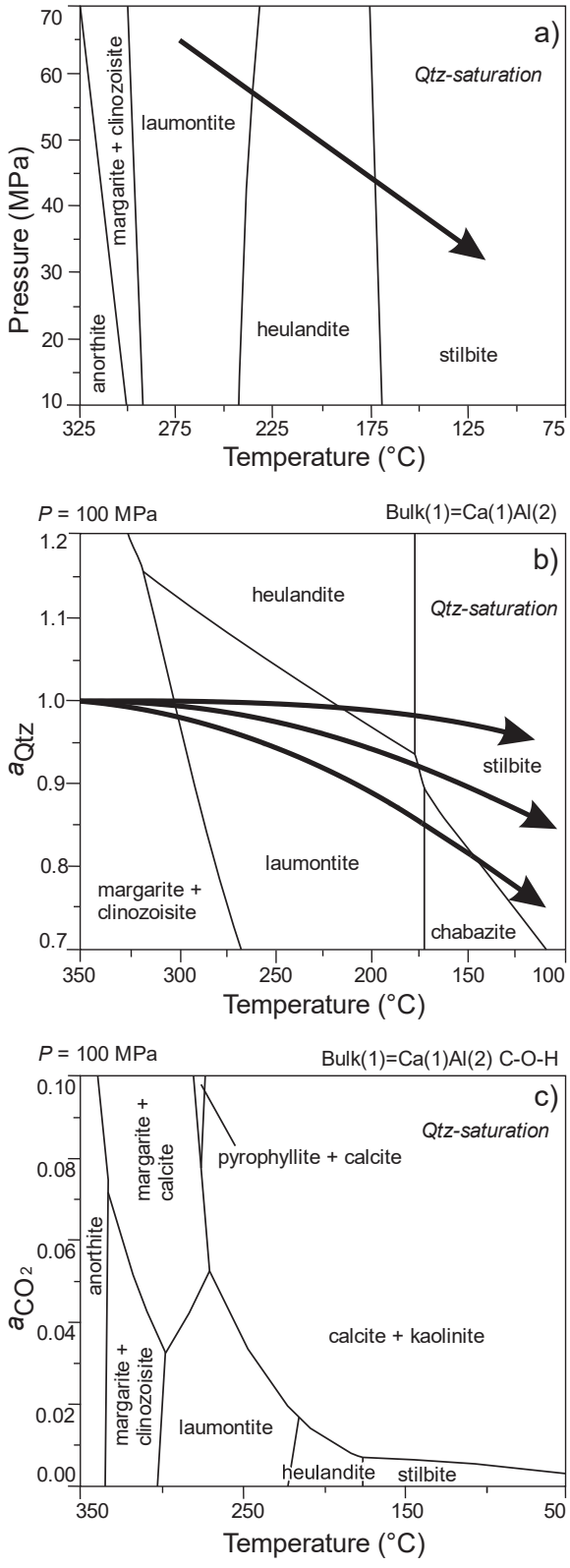

Fig. 1 Assemblage stability diagram in the Ca-Al-Si-O-H system at P = 100 MPa (Weisenberger and Bucher 2010); **a** – P–T diagram, **b** – $a\mathrm{SiO_2}$–T diagram, **c** – $a\mathrm{CO_2}$–T diagram. The arrow is a retrograde cooling path in the Alpine-type hydrothermal veins from the Alps (Mullis et al. 1994).

U-mines of the Rožná–Olší ore field obtained during mining activities were taken from the Moravian Museum and they were often donated by the coauthors (DŠ, JM). They collected these mineral samples despite the internal rules which strictly prohibited collection of any minerals and rocks in the U-mines, which were valid up to the early 1990ies. All abbreviations of minerals were used according to Warr (2021).

3.2. Chemical composition

Chemical analyses of studied phases were performed on carbon-coated epoxy mounts using a Cameca SX-100 electron-probe microanalyzer in wavelength-dispersive mode. The following analytical conditions were used for zeolites (and other phases): accelerating voltage of 15 kV, beam current of 4 nA (10 nA), and beam diameter of 10 μm (5 μm). Following natural and synthetic standards were used for quantification: albite (Na), sanidine (K, Al, Si), pyrope, (Mg), almandine Fe, spessartine (Mn); wollastonite (Ca), titanite (Ti), topaz (F), vanadinite (Pb, Cl), Ni_2SiO_4 (Ni), gahnite (Zn), baryte (Ba), $SrSO_4$ (Sr). Peak counting times (CT) were 10 s for main elements and 20–40 s for minor elements; CT for each background was one-half of the peak CT. The raw intensities were converted to the concentrations using X-PHI (Merlet 1994) matrix-correction software involving the theoretical amount of unanalyzed oxides in the correction routine.

Coefficients of empirical formulas were calculated on the basis of 6 oxygen atoms (pollucite, analcime), 32 oxygen atoms [phillipsite-(Ca), harmotome], 24 oxygen atoms [chabazite-(Ca,K)], 48 oxygen atoms (laumontite), 10 oxygen atoms (natrolite, scolecite), 72 oxygen atoms [stilbite-(Ca), heulandite-(Ca)], 20 oxygen atoms [thomsonite-(Ca)] and according to the idealized compositions (Coombs et al. 1997). The composition of the base tetrahedra zeolites is expressed by the ratio T_{si} = Si/Si + Al (Tschernich 1992). In addition, a measure of charge balance was calculated on the basis of the formula $E\% = 100 \times [(Al + Fe^{3+}) - (Li + Na + K) - 2(Ca + Mg + Sr + Ba)] / [(Li + Na + K) + 2(Ca + Mg + Sr + Ba)]$ (Passaglia 1970; Deer et al. 2004).

3.3. Raman spectroscopy

Zeolites of mm to μm size grains were analyzed by Raman spectroscopy from polished sections, where X-ray diffraction is not possible or very complicated. This method was used as a supplementary technique to the WDS analysis to confirm the structural identification. The Raman spectra of zeolites were obtained by means of a Horiba Labram HR Evolution spectrometer. This dispersive, edge-filter-based system is equipped with an Olympus BX 41 optical microscope, a diffraction grating

with 600 grooves per millimeter, and a Peltier-cooled, Si-based charge-coupled device (CCD) detector. After careful tests with different lasers (473, 532 and 633 nm), the 633 nm He-Ne laser with the beam power of 5 mW at the sample surface was selected for spectra acquisition to minimize analytical artifacts. Raman signal was collected in the range of 100–4000 cm^{-1} with a 100× objective (NA 0.9), and the system being operated in the confocal mode, beam diameter was ~1 μm and the depth resolution ~2 μm. No visual damage of the analyzed surface was observed at these conditions after the excitation. Wavenumber calibration was done using the Rayleigh line and low-pressure Ne-discharge lamp emissions. The wavenumber accuracy was ~0.5 cm^{-1}, and the spectral resolution was ~2 cm^{-1}. Band fitting was done after appropriate background correction, assuming combined Lorentzian–Gaussian band shapes using the Voight function.

4. Results

4.1. Paragenetic and textural types of zeolite mineralizations and sequences of crystallization on tectonic fractures and fissures

We recognized several types of zeolite mineralizations that are distinct in: 1) their geological position (host rock, ductile to brittle and brittle tectonic fractures and fissures), 2) the degree of host rock hydrothermal alterations, 3) the textural development of zeolites including the presence of open vugs (pockets) with crystals of zeolites, 4) their mineral assemblages and parental medium (see Tab. 1). Also, regional distribution of the zeolite mineralizations within the Strážek Unit was examined (Fig. 2).

4.1.1. Granitic pegmatites (A)

Zeolites are typical minerals in granitic pegmatites situated exclusively along the eastern border of the Strážek Unit (Fig. 2) – Věžná I, Věžná II, Drahonín VI (Černý 1960, 1965a, b; Teertstra et al. 1995; Pauliš and Cempírek 1998; Dosbaba and Novák 2012; Toman and Novák 2018; Gadas et al. 2016, 2020; Čopjaková et al. 2021) and Domanínek (Tab.1); they are typically enclosed in serpentinites or Fe-skarn (ESM 1). Paragenetic position of zeolites in the evolution of the individual pegmatite dikes are very different (see for details below) and they are volumetrically negligible within all pegmatite bodies.

(A1) The complex assemblage pollucite + analcime + harmotome + chabazite-(Ca) from the albite–pollucite unit at the Věžná I pegmatite (Tab. 1, 2; Fig. 3a,b) is unique (Teertstra et al. 1995; Toman and Novák 2018). The pollucite-dominant assemblage is developed as a nodular aggregate, ~3 cm in size, with rare small

Tab. 1 Paragenetic types of zeolite mineralizations in the region.

Textural-paragenetic type	locality/dominant zeolite at several localities	genetic or textural type	tectonic position	alteration of host rock/minerals	open vug	typical zeolites	source
A	**Pegmatites, Strážek Unit**						
A1	Věžná I	late magmatic to hydrothermal		moderate	rare	pollucite, analcime, harmotome, chabazite-(Ca)	1
A2	Věžná I, Věžná II, Drahonín VI	pseudomorphs		strong	rare	phillipsite-(Ca) to harmotome, chabazite-(Ca), natrolite	1,2,3
A3	Věžná II	hydrothermal veinlets	brittle fissures	strong to moderate	absent to rare	thomsonite-(Ca), phillipsite-(Ca) to harmotome	1,4,5,6
	Domanínek			weak	absent	laumontite	
B	**Alpine-type hydrothermal veins, Strážek Unit**						
B1	Mirošov	retrograde Alpine-type hydrothermal veins	ductile to brittle fractures	strong	typical	stilbite-(Ca)	7,8
	Pikárec					stilbite-(Ca)	
B2	laumontite/10 localities	hydrothermal veinlets	brittle fissures	weak	absent	laumontite	
B3	natrolite/3 localities					natrolite	
C+D	**Hydrothermal, Rožná U-deposit**						
C	Dolní Rožínka-Jasan 16th level	hydrothermal veins	ductile to brittle fractures	strong	typical	stilbite-(Ca), heulandite-(Ca)	9,10
D	Dolní Rožínka, Bukov	hydrothermal veinlets	brittle fissures	weak to none	typical	harmotome	10,11

Sources: 1 – Toman and Novák (2018), 2 – Čopjaková et al. (2021), 3 – Gadas et al. (2020), 4 – Dosbaba and Novák (2012), 5 – Černý (1965a), 6 – Pauliš and Cempírek (1998), 7 – Černý (1955), 8 – Vávra (1997), 9 – Šťáva (1981), 10 – Pauliš and Šikola (1999), 11 – Uhlík and Řídkošil (1987).

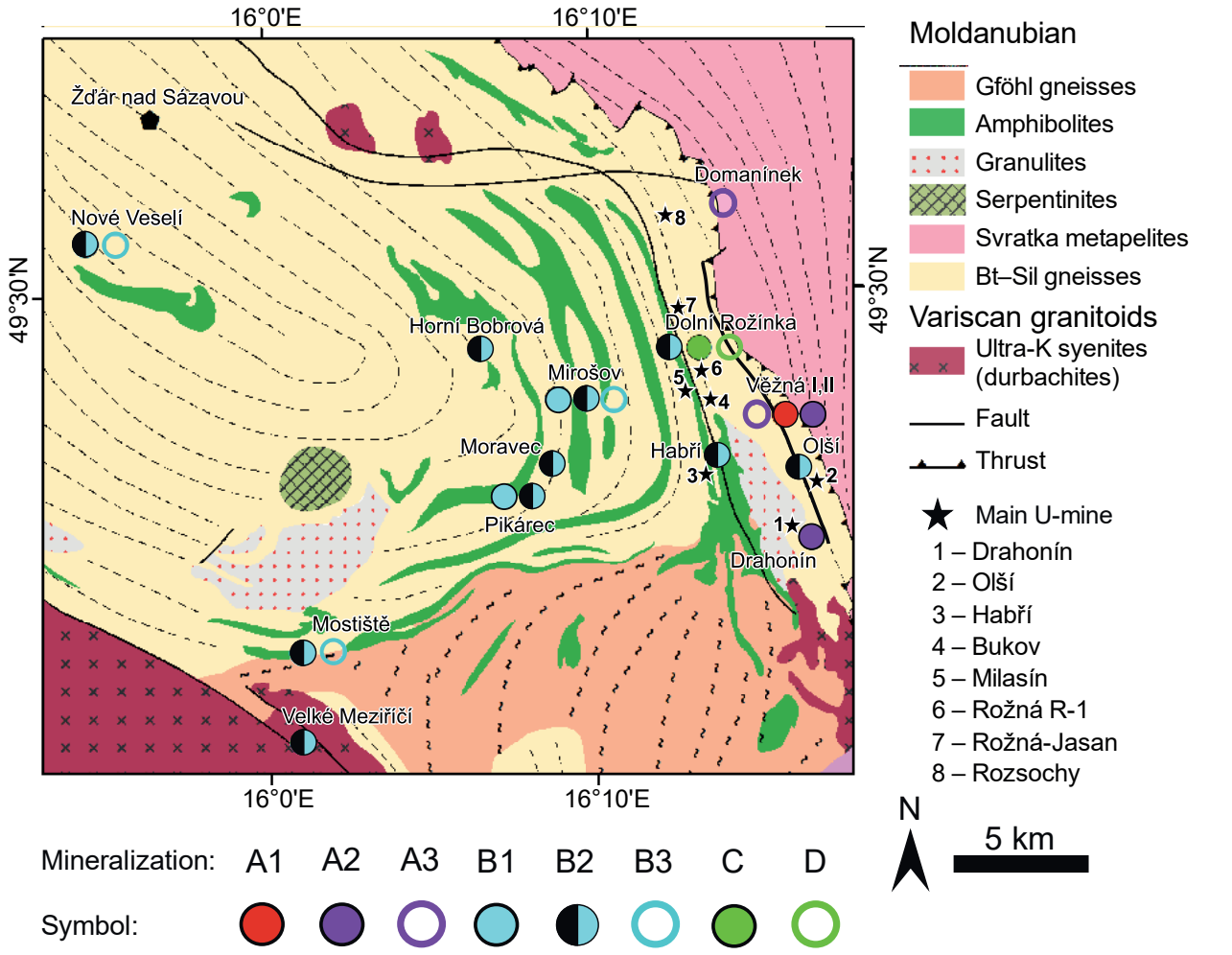

Fig. 2 Schematic geological map of the Strážek Unit with the examined localities of zeolite mineralizations.

pockets typically located along the contact of the pollucite nodule with the host albite-rich portion of the most evolved albite–pollucite unit (Fig. 3a). Primary zeolites (mainly pollucite) in the nodule likely crystallized from the center to the edge where small pockets with crystals of chabazite-(Ca) and harmotome are developed (Fig. 3a, c); pollucite has not been observed in these pockets. Polylithionite, sokolovaite, K-feldspar and elbaite crystallized within the same pocket in the opposite direction from the host pegmatite unit (Fig. 3c). Its origin signifies the latest stage of primary magmatic crystallization and subsequent hydrothermal processes generated analcime after pollucite I in the first step, and the assemblage pollucite II + chabazite-(Ca) + harmotome in the next steps (Fig. 3b; for more details see Toman and Novák 2018).

Two texturally distinct types of hydrothermal zeolite assemblages were identified in the granitic pegmatites; (A2) minor to accessory minerals within pseudomorphs after primary magmatic minerals are very rare, whereas (A3) crystals and aggregates on brittle tectonic fissures are common.

(A2) Zeolites in pseudomorphs (except for analcime + chabazite-(Ca) + harmotome after pollucite described above) include several mineral assemblages where zeolites are typically present in minor to trace amounts: kerolite >> celadonite + albite + adularia > pectolite + natrolite + analcime after quartz in the outermost pegmatite units (Věžná I; Dosbaba and Novák 2012); smectite > harmotome as a late stage replacement of Be-cordierite with common early subsolidus assemblage muscovite + chlorite + phlogopite + beryl + dravite (Věžná I; Gadas et al. 2020); chlorite, muscovite > natrolite after dravitic tourmaline (Drahonín VI; Čopjaková et al. 2021).

(A3) The fissure-filling assemblages are developed especially in the pegmatites Věžná II and Domanínek. They include a rather common thomsonite-(Ca) or phillipsite-(Ca) to harmotome (Fig. 3d,e,f), ongrowing strongly altered oligoclase or secondary prehnite after oligoclase, rare natrolite on relatively fresh albite (Černý 1965b) and rare chabazite-(K) associated with harmotome (Pauliš and Cempírek 1998). At the pollucite assemblages from Věžná I, late magmatic to hydrothermal continuous

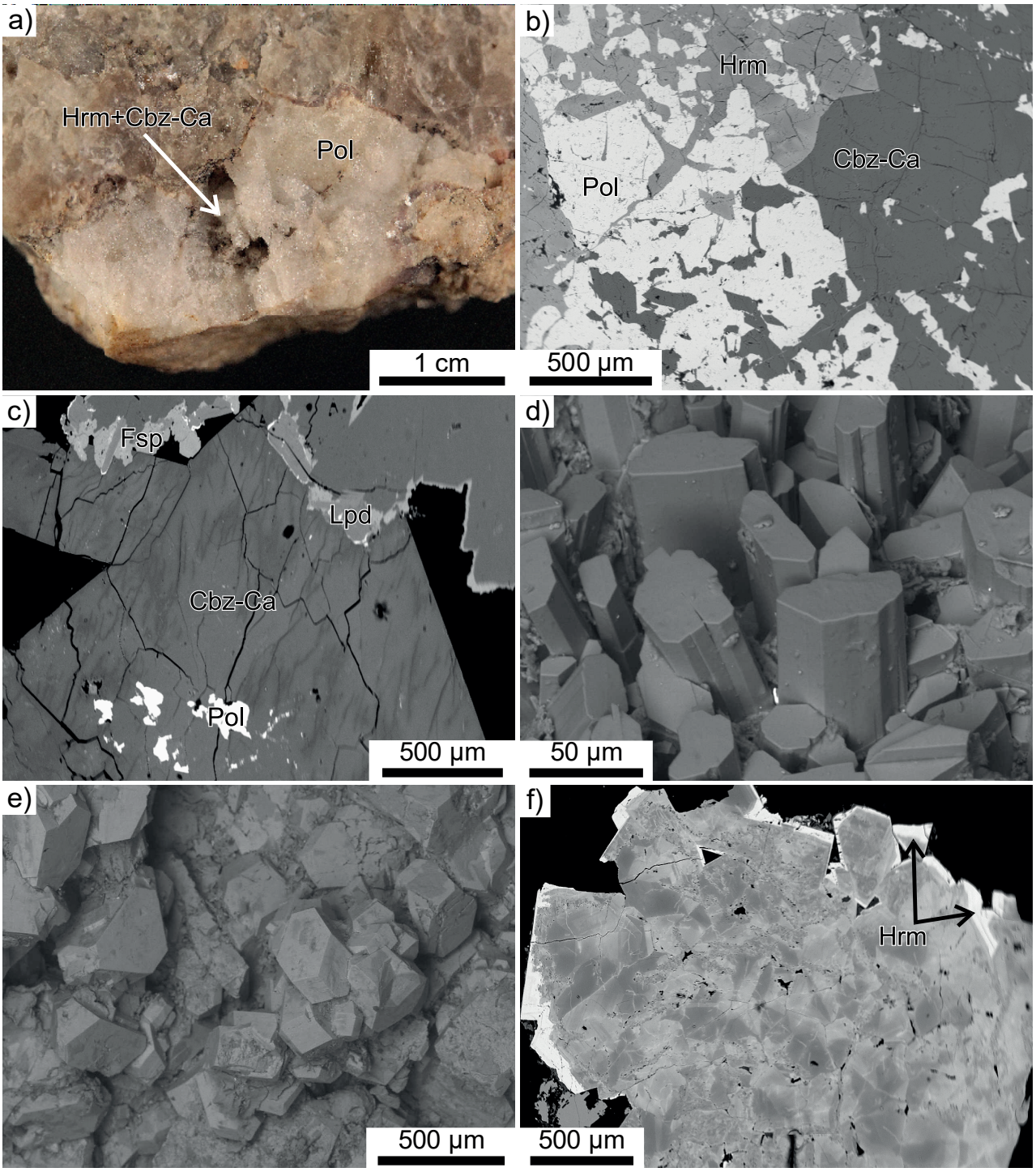

Fig. 3 Photographs, BSE and SEM images of zeolites from granitic pegmatites (A): **a –** the assemblage pollucite + harmotome + chabazite-(Ca) rimmed by flakes of violet lepidolite from albite–pollucite unit; **b –** the assemblage pollucite (Pol) + harmotome (Hrm) + chabazite-(Ca) (Cbz-Ca) (A1); **c –** pocket adjacent to albite–lepidolite aggregate, with the crystal of chabazite-(Ca) replaced by dark veinlets of Mg-enriched chabazite-(Ca) (A2), **a, b, c –** Věžná I; **d –** thomsonite-(Ca) crystals on fissure; **e –** phillipsite-(Ca)–harmotome crystals on fissure; **f –** sectorial zoning in phillipsite-(Ca) with bright rims of harmotome, **d, e, f –** (A3), Věžná II.

and complex process was terminated by microscopic fissure fillings of Mg-enriched chabazite-(Ca) cutting and replacing crystals of early chabazite-(Ca) (Fig. 3c, Tab. 2; Toman and Novák 2018). Laumontite overgrowing early secondary prehnite after oligoclase is common on brittle fractures from sub-homogeneous, coarse-grained con-

Tab. 2 Description of the individual paragenetic types of zeolite mineralizations.

	locality or dominant zeolite at several localities	host or replaced rock/mineral	max. size of crystals	zeolites	typical associated minerals
A1	Věžná I	albite–pollucite unit	mm	pollucite, analcime, chabazite-(Ca), harmotome	lepidolite, triplite, albite, apatite, elbaite, topaz
A2	Věžná I, Věžná II, Drahonín VI	cordierite, quartz, oligoclase, prehnite, tourmaline	μm	phillipsite-(Ca) to harmotome, natrolite, analcime, Mg-rich chabazite-(Ca)	kerolite, pectolite, smectite, adularia, chlorite, muscovite
A3	Věžná II	oligoclase, albite, prehnite	mm to μm	thomsonite-(Ca), phillipsite-(Ca) to harmotome > natrolite	prehnite, calcite
	Domanínek	prehnite	cm	laumontite	prehnite
B1	Mirošov	amphibolite	cm	stilbite-(Ca) > chabazite-(K), heulandite-(Ca)	quartz, epidote, axinite, prehnite
	Pikárec	amphibolite	mm	stilbite-(Ca) > chabazite-(Ca), laumontite	epidote, prehnite, ferro-edenite
B2	laumontite/10 localities	various rocks	mm	laumontite	prehnite, adularia,
B3	natrolite/3 localities	various rocks	mm	natrolite, analcime > laumontite, scolecite	prehnite, epidote
C	Dolní Rožínka-Jasan 16th level	calc–silicate rock	cm	stilbite-(Ca), heulandite-(Ca) >> chabazite	pyrite, titanite, apophyllite
D	Dolní Rožínka, Bukov	various rocks	mm	harmotome	calcite

taminated pegmatite (Kfs + Pl + Hbl + Qz ± Flr, Aln-Ce). Its dikes, up to 0.5 m thick, discordantly cut Fe-skarn at Domanínek near Bystřice nad Pernštejnem (Fig. 2).

4.1.2. Alpine-type hydrothermal veins and veinlets (B)

Three distinct types of Alpine-type hydrothermal veins to thin veinlets with zeolites were found in the Strážek Unit. They are distributed in the majority of the region, including Rožná-Olší ore field (Fig. 2), and were described from quarries in amphibolite bodies (e.g., Mirošov, Nové Veselí) or collected during the drilling program (Pikárec). Zeolites are also known from dumps of U-mines and other prospection and mining activities in this region (Kruťa 1966).

(B1) Classic Alpine-type hydrothermal veins are characterized mainly by the occurrence of crystals developed in open vugs of tectonic fractures in amphibolites. A strong hydrothermal alteration of host rocks developed along vein borders is typical (Vávra 1997) as well as a ductile to the brittle character of most mineralized fractures. The size/thickness of open space is variable from ~5 mm to ~2 dm and crystals of quartz may achieve up to 15 cm in size at the Alpine-type veins from the Mirošov quarry (Fig. 4a; Černý 1955; Vávra 1997). The veins from Mirošov have variable mineral assemblages, with quartz and epidote as the earliest minerals, along with axinite-(Fe), prehnite, albite, adularia, and chlorite. Zeolites (heulandite-(Ca), stilbite-(Ca), chabazite-(K)) are typically the latest minerals overgrowing earlier formed minerals (Fig. 4a). A very similar assemblage with dominant epidote + prehnite + zeolites is developed in the vein, up to 5 cm thick, enclosed in altered amphibolite from the drill-hole P1, depth 157.3 m in Pikárec (Fig. 2, Tab. 2). Laumontite, stilbite-(Ca) and chabazite-(Ca) were identified in open vugs along with early epidote and prehnite (Tab. 1, 2; Fig. 4b). Alpine-type veins with prehnite, chlorite, and axinite-(Fe) occur in the Rožná U-deposit, the Jasan Mine, 20th and 22nd level (Pauliš and Šikola 1999); however, no zeolites have been found in this assemblage.

(B2) Laumontite veinlets (10 localities; ESM 1) and (B3) natrolite veinlets (Mostiště, Nové Veselí, Mirošov), typically < ~1–2 mm thick, occur in thin, brittle fractures within fine- to medium-grained amphibolites or biotite gneiss in Velké Meziříčí (ESM 1) which typically cut foliation of host rock. No open vugs are developed in fissures and hydrothermal alteration of host rocks is weak. Along with laumontite, rare early epidote, and/or prehnite, and adularia were identified in some veinlets (Fig. 4c,d; Tab. 2). The examined localities include Mirošov, Moravec, Pikárec, Nové Veselí, Velké Meziříčí, Mostiště, Horní Bobrová (Fig. 2) and laumontite localities are also situated in the Rožná–Olší ore field (e.g., Habří, Dolní Rožínka and Olší; Burkart 1953; Kruťa 1966). The (B3) rare natrolite veinlets differ in the overall mineral assemblages and abundance of Na-zeolites: natrolite (Mirošov), prehnite + laumontite + natrolite + analcime (Nové Veselí), epidote + prehnite + natrolite + scolecite (Mostiště) (Fig. 4e,f). The mutual relations of the laumontite and natrolite veinlets are not known.

4.1.3. Zeolite assemblages from the Rožná–Olší ore field (C, D)

Two types of zeolite-dominant assemblages distinct in textures (ductile to brittle or brittle character of fractures), degree of alteration of host rocks and mineral assemblages were recognized within the Rožná–Olší ore field (Tab. 1, 2): (C) stilbite-(Ca)-dominant hydrothermal

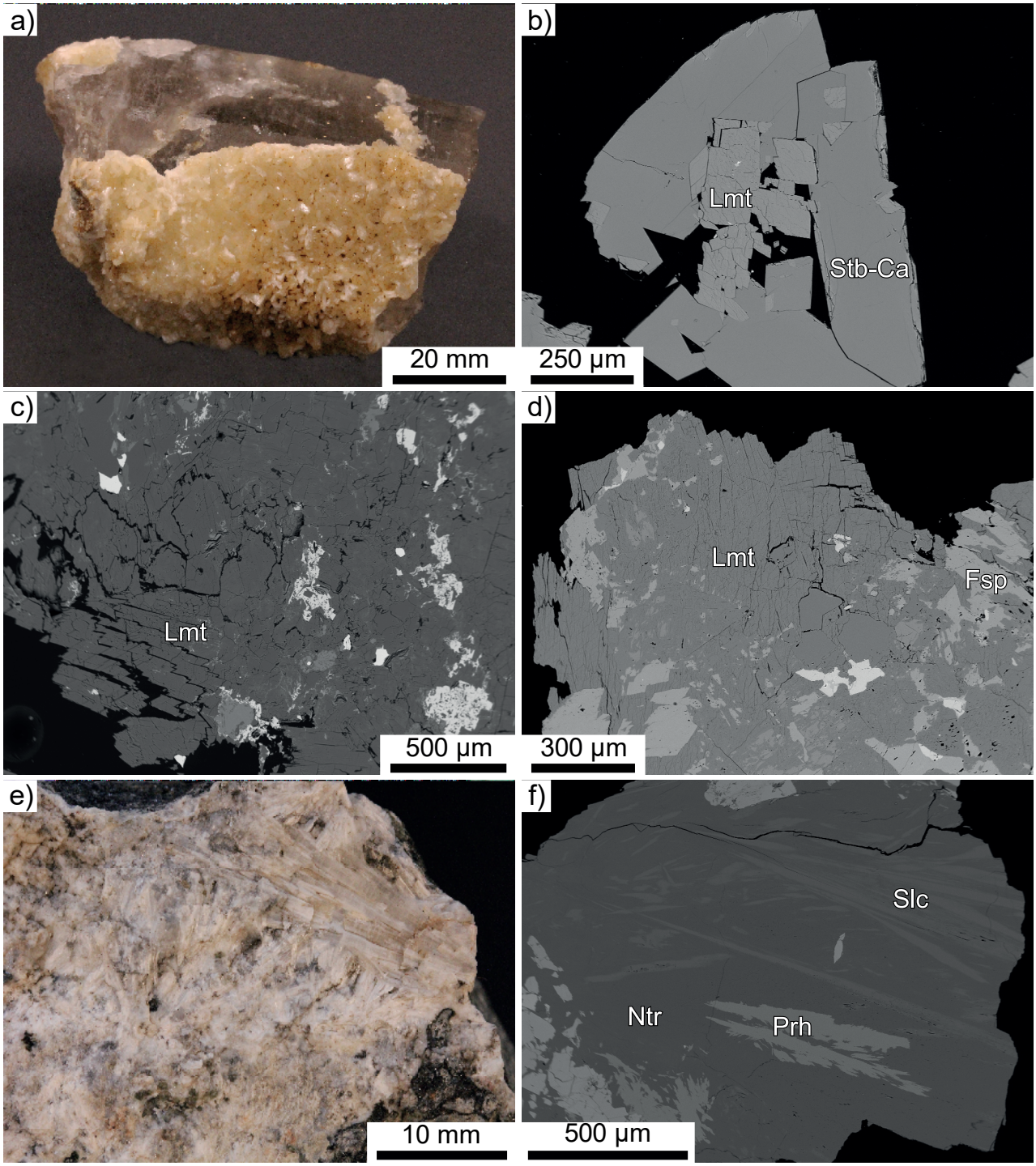

Fig. 4 Photographs and BSE images of zeolites from Alpine-type veins (B): **a –** stilbite-(Ca) overgrowing large quartz crystal – Mirošov (B1); **b –** stilbite-(Ca) (Stb-Ca) crystals overgrowing laumontite (Lmt) – Pikárec (B1); **c** and **d –** fissure-filling laumontite (Lmt) associated with adularia (Fsp) – Mirošov, Mostiště (B2); **e –** fissure-filling natrolite + fibrous scolecite; **f –** fissure-filling natrolite (Ntr) with lamellae of scolecite (Slc) and aggregate of prehnite (Prh); **e, f –** Mostiště (B3).

veins with strong alteration of the host rock (Šťáva 1981) and thin (D) harmotome fissure-filling veinlets with no to weak alteration of host rocks (Tab. 1, 2). Both assemblages typically contain common open vugs.

(C) Stilbite-(Ca)-dominant hydrothermal veins exhibit textural features similar to the Alpine-type hydrothermal veins (B1) – strong alteration of the host rock, presence of open vugs and ductile to brittle character of fractures;

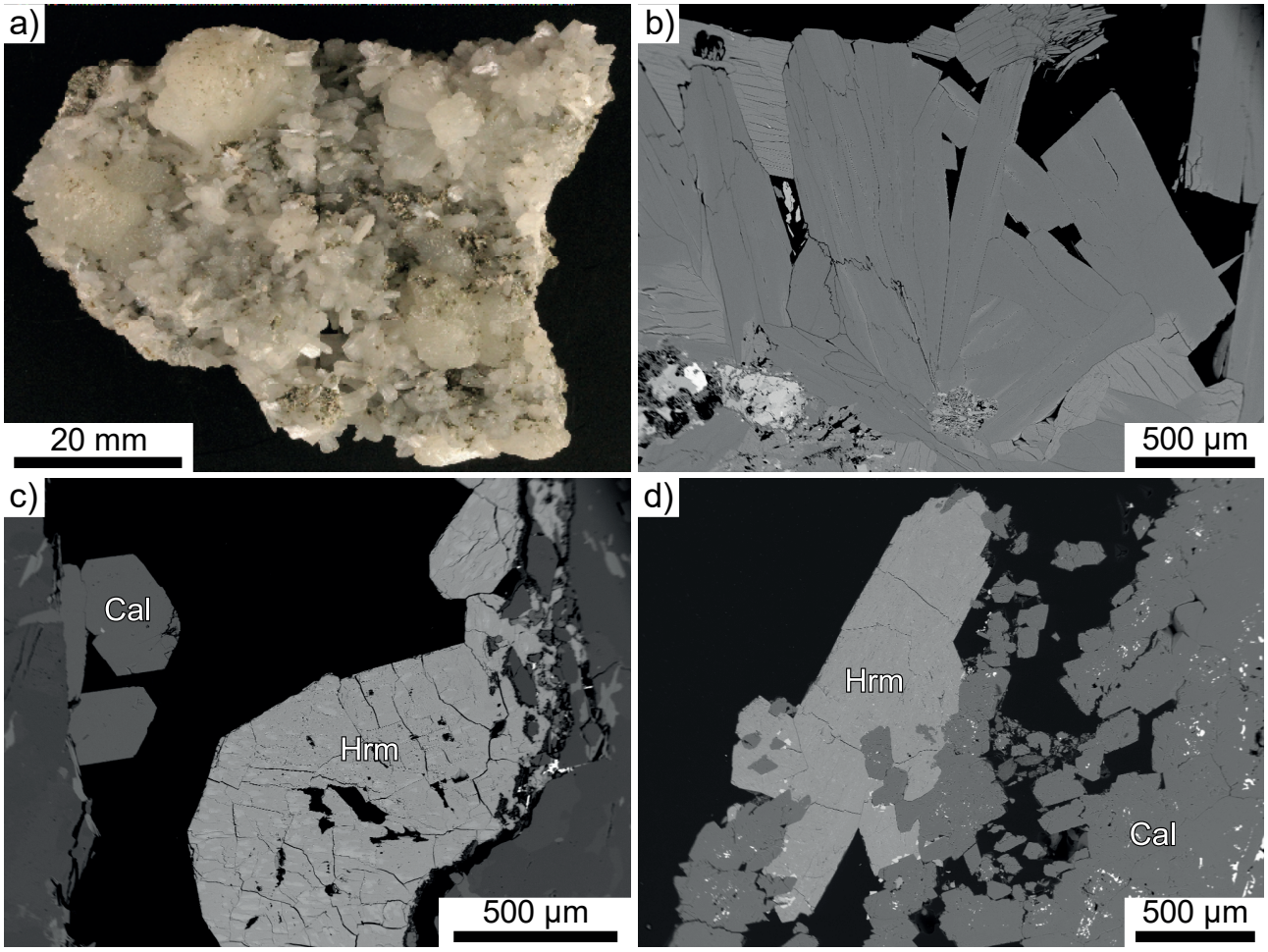

Fig. 5 Photographs and BSE images of fissure-filling zeolites and from pockets in hydrothermal veins, Rožná U-deposit, (C, D): **a –** crystals of stilbite-(Ca) in pocket from the stilbite veins; **b –** crystals of stilbite-(Ca) (C); **c** and **d –** harmotome crystals and associated early calcite on fissure, note weak alteration of the host rock (D).

however, they differ in the absence of typical high-T minerals (epidote, prehnite), the dominance of zeolites (Tab. 2) and their host rocks. They were described from the Jasan Mine, 16th level, (Šťáva 1981; Pauliš and Šikola 1999) as very common radial aggregates of stilbite-(Ca), up to 3 cm in diameter, associated with early heulandite-(Ca) and rare chabazite, titanite and common pyrite in pockets (Fig. 5a,b). Host amphibolite and calc-silicate rock (Hbl + Pl + Di + Adr + Ab + Py + Qz) locally with thin calcite marble interlayers (< 5 mm thick) show strong to moderate alterations. Common pyrite and accessory pyrrhotite, chalcopyrite and microscopic NiS_2 phase are typical.

(D) Harmotome fissure-filling veinlets are the most widespread zeolite mineralization within the Rožná-Olší ore field (Pauliš and Šikola 1999). Veinlets on brittle fissures are mostly thin (≤~1–3 mm) and typically with open vugs. They are always discordant to the foliation of the host rock (biotite gneiss, migmatite, coarse hydrothermal calcite) and alteration of host rocks is weak to none except for dissolved calcite (Fig. 5c). Harmotome forms colorless, white to greyish crystals and their intergrowths, 1–2 mm in size. Colorless crystals of calcite, < 2 mm in size, are often growing on fissure walls (Fig. 5c, d), whereas pyrite is absent or very rare.

The individual zeolite assemblages mostly show recognizable crystallization sequences. In the Věžná I pegmatite, the sequence early chabazite-(Ca) → Mg-rich chabazite-(Ca) in microscopic fissures (Fig. 3c). On fissures (A3) from Věžná II, a sole zeolite (thomsonite or natrolite) is mostly present and zoned crystals of phillipsite show sequence phillipsite-(Ca) → harmotome (Fig. 3f). (B1) The Alpine-type hydrothermal veins have the crystallization sequence: epidote → prehnite → zeolites at most localities; late zeolites are only scarcely in a direct contact within small open vugs and only the sequences: laumontite → stilbite-(Ca) (Fig. 4b), and stilbite-(Ca) → chabazite-(Ca) were observed. (B2) The sequences prehnite → laumontite, epidote → laumontite, were recognized in the laumontite veinlets and prehnite →

natrolite in the (B3) natrolite veinlets. The textural relation of intergrowths natrolite + scolecite (Fig. 4f) is not clear. (C) In the stilbite veins from the Jasan Mine, 16th level, the sequence heulandite-(Ca) → stilbite-(Ca) → chabazite-(Ca) (Šťáva 1981) is apparent; common pyrite crystallized from early to late stages. (D) Fissure-filling veinlets contain harmotome and locally also calcite (Fig. 5c,d) and both sequences calcite → harmotome (Fig. 5d) and harmotome → calcite were observed. All observed crystallization sequences, including zeolites are in line with the experimental results (Fig. 1).

4.2. Geological environments of the individual zeolite mineralizations and their regional distribution

The assemblage pollucite + chabazite-(Ca) + harmotome (A1) forms an oval aggregate enclosed within the albite-pollucite unit, the most evolved primary unit of the Věžná I pegmatite (for more details, see Toman and Novák 2018). Minor to accessory zeolites from pseudomorphs after primary minerals (A2) are rather randomly distributed within dominant secondary phases (e.g., prehnite, kerolite, muscovite, smectite, and/or chlorite). Their textural relations to other secondary minerals in pseudomorphs are commonly ambiguous, but in some assemblages, zeolite is the latest phase (Čopjaková et al. 2021).

Other zeolite mineralizations (A3, B1, B2, B3, C, D) occur on tectonic fractures or fissures within host rock or mineral and several distinct types were recognized. The (B1) Alpine-type hydrothermal veins and the (C) stilbite veins from the Jasan Mine are characterized by rather large open vugs, up to 1–2 dm in size, locally with large crystals (Fig. 4a, 5a), and mainly by the transitional ductile to brittle character of these mineralized fractures. Alteration of host rocks is typical in both types but stronger at the Alpine-type hydrothermal veins (B1) with abundant epidote. Zeolites typically overgrow early minerals (Fig. 4a) and no replacement textures, as well as late brittle tectonic fissures filled by zeolites associated with the (B1) and (C) mineralizations, were observed.

The thin veinlets (A3, B2, B3, D) on brittle fractures and fissures are typically discordant to the foliation or banding of host rock and alteration of the host rock is typically weak (A3, B2, B3) to none (D). The hydrothermal laumontite- and natrolite-dominant veins (B2, B3) differ by the total absence of open vugs, which are typical for the harmotome fissure-filling veinlets (D) (Fig.5c,d) and rare to common on fractures from the Věžná II pegmatite (Fig. 3d,e).

Zeolites from granitic pegmatites (A) are enclosed in a variety of replaced primary minerals and textural-paragenetic units (Tab. 2) and were not discussed in detail. All types of Alpine-type hydrothermal veins (B1, B2, B3) almost exclusively cut fine- to medium-grained amphibolites and only the laumontite vein (B2) from Velké Meziříčí cuts biotite gneiss. Both zeolite mineralizations from the Rožná–Olší ore field differ significantly. The stilbite veins (C) are enclosed in heterogeneous/banded calc-silicate rock with intercalations of amphibolite and calcite marble, whereas the harmotome veinlets (D) cut discordantly variety of rocks and minerals, including biotite gneiss, migmatite and coarse-grained hydrothermal calcite with the altered surface (ESM 1).

Alpine-type hydrothermal veins (B1) with epidote, prehnite and zeolites, as well as thin laumontite (B2) and rare (B3) natrolite veinlets are distributed within the whole studied region (Fig. 2). They occur almost exclusively in amphibolites (ESM 1) and absence of zeolites in some NW-located areas (Fig. 2) may be caused by the absence of suitable rock outcrops in the flat landscape. (A) Zeolites from granitic pegmatites (Věžná I, Věžná II, Drahonín VI, Domanínek) occur exclusively along the eastern border of the Strážek Unit, and east of the Rožná–Olší ore field. In abundant granitic pegmatites from the Strážek Unit no zeolites have been discovered (e.g., Gadas et al. 2012; Novák et al. 2015a, b), including elbaite pegmatite from Dolní Rožínka (Novotný et al. 2019) and lepidolite pegmatite Drahonín I both latter located W of the shear zones Rožná and Olší, respectively. The zeolite assemblages – (C) hydrothermal veins with dominant stilbite-(Ca) and (D) harmotome fissure-filling veinlets are restricted to the Rožná–Olší ore field (Fig. 2) and all were collected during active mining. The stilbite veins are known solely from the Jasan Mine, 16th level (Šťáva 1981), whereas the harmotome veinlets are more widespread from 5th to 22nd level mainly on the U-mines – R1, Jasan and Bukov (Pauliš and Šikola 1999). No zeolites are known from the Svratka Crystalline Complex adjacent to the Strážek Unit.

4.3. Chemical composition of the individual zeolites

Chemical compositions of zeolites were obtained using EPMA (Tab. 3a,b, 4a,b, 5). The contents of H_2O were calculated by difference so that the oxide totals in zeolites are 100 % and were not discussed in detail. The identification of some zeolites was confirmed using Raman spectroscopy.

Pollucite (A1) contains low to moderate contents of Na (0.14–0.41 *apfu*) and K close to the detection limit (Toman and Novák 2018). **Analcime** (A1) replacing pollucite is enriched in Cs (≤0.26 *apfu*), whereas (A2) analcime samples from kerolite pseudomorphs at the Věžná I pegmatite (Tab. 3a,b; Dosbaba and Novák 2012) have variable Si/Al ratio (2.06–2.13) similar to analcime (B3)

Tab. 3a Representative chemical analyses of zeolites from granitic pegmatites (A1).

Mineralization	A1									
Locality	Věžná I									
Zeolite	Hrm	Hrm	Hrm	Cbz-Ca	Cbz-Ca	Cbz-Ca	Pol	Pol	Pol	Anl
SiO_2 (wt.%)	51.39	49.84	50.77	56.36	55.91	57.41	45.24	47.00	45.53	56.22
Al_2O_3	18.27	18.05	18.33	19.19	18.99	19.37	16.16	16.70	15.91	19.72
CaO	1.26	1.16	0.77	8.92	8.52	8.32	bdl	bdl	bdl	0.07
BaO	20.53	19.91	20.95	1.22	0.54	0.87	bdl	bdl	bdl	bdl
SrO	bdl	bdl	bdl	0.29	0.46	0.27	bdl	bdl	bdl	bdl
FeO	bdl	bdl	bdl	bdl	bdl	bdl	bdl	bdl	bdl	bdl
MgO	bdl	bdl	bdl	bdl	bdl	0.33	bdl	bdl	bdl	bdl
K_2O	1.83	1.31	0.94	2.53	3.65	2.17	bdl	bdl	bdl	0.25
Na_2O	0.50	0.26	0.43	0.20	0.19	0.22	2.25	3.26	2.12	10.82
Cs_2O	bdl	bdl	bdl	bdl	0.18	bdl	31.81	28.20	32.01	1.66
P_2O_5	bdl	bdl	bdl	bdl	bdl	bdl	0.25	0.24	0.24	0.28
F	bdl	bdl	bdl	bdl	bdl	bdl	0.07	0.07	0.08	bdl
H_2O*	6.22	9.47	7.81	11.29	11.56	11.04	4.22	4.53	4.11	10.98
∑ oxide	100.00	100.00	100.00	100.00	100.00	100.00	100.00	100.00	100.00	100.00
Si (*apfu*)	11.244	11.240	11.264	8.533	8.523	8.579	2.108	2.109	2.114	2.122
Al	4.710	4.798	4.793	3.424	3.412	3.411	0.887	0.883	0.871	0.877
∑ T	15.954	16.038	16.057	11.957	11.935	11.990	2.995	2.992	2.985	2.999
Ca	0.291	0.278	0.181	1.428	1.374	1.315	—	—	—	0.003
Ba	1.761	1.759	1.822	0.072	0.032	0.051	—	—	—	—
Sr	—	—	—	0.026	0.041	0.023	—	—	—	—
Fe	—	—	—	—	—	—	—	—	—	—
Mg	—	—	—	—	—	0.073	—	—	—	—
K	0.511	0.378	0.265	0.488	0.709	0.414	—	—	—	0.012
Na	0.213	0.115	0.186	0.057	0.056	0.062	0.203	0.284	0.191	0.792
Cs	—	—	—	—	0.012	—	0.632	0.540	0.634	0.027
P	—	—	—	—	—	—	0.010	0.009	0.010	0.009
F	—	—	—	—	—	—	0.011	0.009	0.012	—
∑ cat	2.776	2.530	2.454	2.071	2.224	1.938	0.856	0.842	0.847	0.843
H_2O	4.543	7.130	5.785	5.706	5.883	5.507	0.656	0.679	0.637	1.384
Si/Al	2.39	2.34	2.35	2.49	2.50	2.52	2.38	2.39	2.43	2.42
T_{Si}	0.70	0.70	0.70	0.71	0.71	0.72	0.70	0.70	0.71	0.71
E%	–2.28	4.80	7.40	–5.26	–6.58	0.59	7.23	7.32	6.10	6.02

Note: *H_2O calculated by difference; bdl = below detection limit

from Nové Veselí (Fig. 6a,b, Tab. 4b). **Natrolite** is close to the ideal formula in most examined samples (A2) and (B3) except for a single sample of natrolite from Mostiště with slightly elevated contents of Ca (0.00–0.16 *apfu*).

Thomsonite-(Ca) from the pegmatite Věžná II (A3) has slightly elevated Si (5.12–5.26 *apfu*) and lower Al (4.72–4.84 *apfu*), Ca (1.75–1.86 *apfu*), Na (0.99–1.10 *apfu*) and traces of Sr (0.04–0.10 *apfu*) (Tab. 3b). **Scolecite** associated with natrolite (B3) shows weak variations in Na/Ca (Fig. 6b). **Laumontite** is compositionally variable and the samples from (B1) the Alpine type vein in Pikárec, (B2) laumontite veinlets and from (B3) natrolite veinlets differ mainly in the concentrations of K (B1 – 0.00 *apfu*, B2 – 0.00–1.03 *apfu*, B3 – 0.26–0.52 *apfu*; Tab. 4a,b; Fig. 6b). These zeolites have rather stable Si/Al ratio (Fig. 6a,b).

Stilbite-(Ca) from both paragenetic types differs significantly; (B1) stilbite-(Ca) from the Alpine type veins in Mirošov and Pikárec is heterogeneous with highly variable in Na (0.00–1.14 *apfu*), K (0.00–0.59 *apfu*) but rather stable Ca (3.97–4.30 *apfu*) and traces of Mg (≤ 0.08 *apfu*). (C) Stilbite-(Ca) from the stilbite vein from the Jasan Mine, 16th level has K always below the detection limit and highly variable Na (0.38–0.97 *apfu*).

Heulandite-(Ca) occurs in the (B1) Alpine type veins from Mirošov, at the (C) stilbite veins from the Jasan Mine, 16th level. It is always dominant in Ca (B1 – 2.61–2.74 *apfu*, C – 2.21–2.82 *apfu*), with significant to minor amounts of K (B1 – 1.24–1.52 *apfu*, C – 0.36–0.59 *apfu*) and Sr (B1 – 0.55–0.70 *apfu*, C – 0.20–0.90 *apfu*), and trace to high Na (B1 – 0.00 *apfu*, C – 0.41–1.31 *apfu*), Ba (B1 – 0.22–0.23 *apfu*, C – ≤ 0.19 *apfu*) and Mg (B1 – 0.00–0.43 *apfu*, C – 0.00–0.28 *apfu*). Heulandite-(Ca) shows also significant variations in Si/Al ratio (B1 – 2.77–2.91, C – 2.88–3.89, Tab. 4a, 5; Fig. 6b,c).

Chabazite-(Ca) (A1) and **Mg-enriched chabazite-(Ca)** (A2) both from the Věžná I pegmatite, (B1)

Tab. 3b Representative chemical analyses of zeolites from granitic pegmatites (A2, A3).

Mineralization	A2									A3					
Locality	Věžná I					Věžná II		Drahonín VI		Věžná II				Domanínek	
Zeolite	Cbz-Ca	Cbz-Ca	Hrm	Anl	Anl	Hrm-Php-Ca	Hrm-Php-Ca	Ntr	Ntr	Thm-Ca	Thm-Ca	Hrm-Php-Ca	Hrm-Php-Ca	Lmt	Lmt
SiO_2 (wt.%)	56.15	55.92	51.01	55.75	55.11	44.64	44.15	47.66	47.78	37.47	38.41	49.13	46.05	51.44	51.95
Al_2O_3	19.23	18.65	17.64	22.19	22.65	20.77	19.38	26.72	26.93	29.90	29.22	16.46	21.82	20.63	20.39
CaO	6.00	7.66	0.52	0.03	0.03	5.99	3.47	bdl	bdl	12.73	12.07	1.21	5.42	12.07	11.86
BaO	0.83	0.66	20.62	bdl	bdl	8.64	16.32	bdl	bdl	0.30	0.11	18.18	12.76	bdl	bdl
SrO	0.27	0.27	bdl	bdl	bdl	bdl	bdl	bdl	bdl	0.78	0.57	bdl	bdl	bdl	bdl
FeO	bdl	bdl	bdl	bdl	bdl	bdl	bdl	bdl	bdl	bdl	bdl	bdl	bdl	bdl	bdl
MgO	1.89	0.67	0.25	bdl	bdl	bdl	bdl	bdl	bdl	bdl	bdl	0.22	bdl	bdl	bdl
K_2O	2.64	3.33	0.80	0.32	0.32	2.39	1.45	bdl	bdl	bdl	0.17	0.52	2.60	0.29	0.33
Na_2O	bdl	0.11	0.99	12.46	13.06	0.15	0.40	16.20	16.50	3.90	4.15	bdl	0.24	bdl	bdl
Cs_2O	bdl	0.08	bdl	bdl	bdl	bdl	bdl	bdl	bdl	bdl	bdl	bdl	bdl	bdl	bdl
P_2O_5	bdl	bdl	bdl	bdl	bdl	bdl	bdl	bdl	bdl	bdl	bdl	bdl	bdl	bdl	bdl
F	bdl	bdl	bdl	bdl	bdl	bdl	bdl	bdl	bdl	0.07	0.09	bdl	bdl	bdl	bdl
H_2O*	12.99	12.65	8.17	9.25	8.83	17.42	14.83	9.42	8.79	14.85	15.21	14.28	11.11	15.57	15.47
∑ oxide	100.00	100.00	100.00	100.00	100.00	100.00	100.00	100.00	100.00	100.00	100.00	100.00	100.00	100.00	100.00
Si (*apfu*)	8.549	8.571	11.329	2.051	2.026	10.397	10.533	3.010	3.002	5.139	5.260	11.506	10.275	16.211	16.315
Al	3.451	3.369	4.617	0.962	0.982	5.702	5.449	1.989	1.994	4.833	4.717	4.544	5.739	7.664	7.547
∑ T	12.000	11.940	15.946	3.013	3.008	16.099	15.982	4.999	4.996	9.972	9.977	16.050	16.014	23.875	23.862
Ca	0.966	1.243	0.123	0.001	0.001	1.476	0.876	—	—	1.846	1.749	0.301	1.278	4.024	3.940
Ba	0.049	0.040	1.795	—	—	0.789	1.526	—	—	0.016	0.006	1.668	1.115	—	—
Sr	0.024	0.024	—	—	—	—	—	—	—	0.062	0.046	—	—	—	—
Fe	—	—	—	—	—	—	—	—	—	—	—	—	—	—	—
Mg	0.429	0.154	0.084	—	—	—	—	—	—	—	—	0.078	—	—	—
K	0.513	0.651	0.226	0.015	0.015	0.711	0.443	—	—	—	0.030	0.154	0.740	0.115	0.133
Na	—	0.034	0.425	0.889	0.931	0.066	0.186	1.984	2.010	1.036	1.103	—	0.105	—	—
Cs	—	0.005	—	—	—	—	—	—	—	—	—	—	—	—	—
P	—	—	—	—	—	—	—	—	—	—	—	—	—	—	—
F	—	—	—	—	—	—	—	—	—	0.030	0.038	—	—	—	—
∑ cat	1.981	2.151	2.653	0.905	0.947	3.042	3.031	1.984	2.010	2.990	2.972	2.201	3.238	4.139	4.073
H_2O	6.602	6.473	6.057	1.136	1.084	13.544	11.812	1.986	1.843	6.798	6.954	11.164	8.275	16.382	16.219
Si/Al	2.48	2.54	2.56	2.13	2.06	1.82	1.93	1.51	1.51	1.06	1.12	2.53	1.79	2.12	2.16
T_{Si}	0.71	0.72	0.72	0.68	0.67	0.65	0.66	0.60	0.60	0.52	0.53	0.72	0.64	0.68	0.68
E%	0.00	–5.87	–5.15	5.49	3.16	7.14	0.00	0.50	–1.00	–1.43	–0.63	6.82	1.59	–6.13	–5.74

Note: *H_2O calculated by difference; bdl = below detection limit

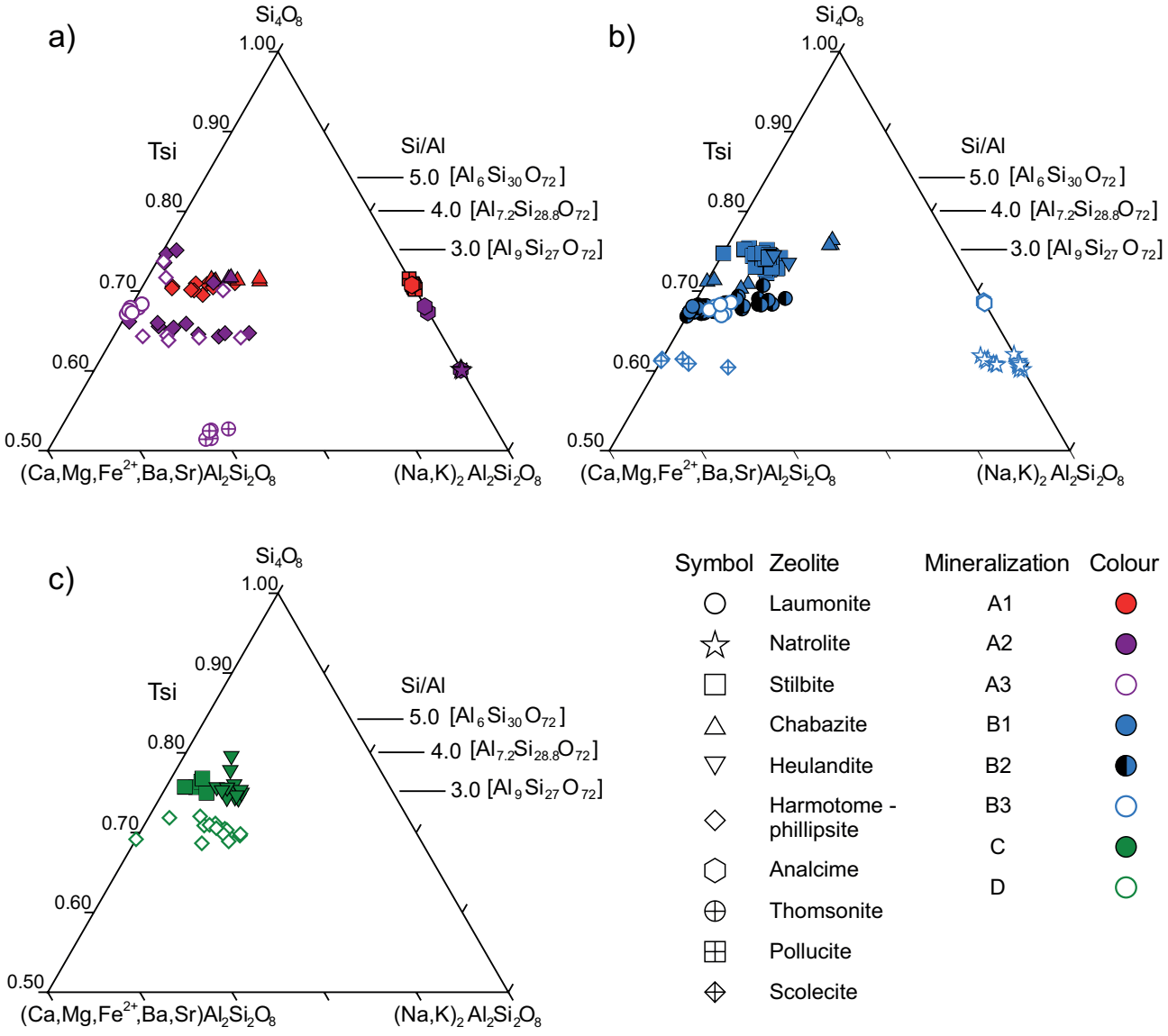

Fig. 6 Diagram Si–R^{2+}AlSi –R^{+}AlSi for the studied zeolites.

chabazite-(K) from Mirošov and **chabazite-(Ca)** from Pikárec are highly variable and contain elevated number of extra-framework cations including Ca (A1 – 1.08–1.43 *apfu*, A2 – 0.97–1.24 *apfu*, B1 – 0.81–0.86 *apfu* (Mirošov) and 1.56–1.68 *apfu* (Pikárec)), K (A1 – 0.41–1.00 *apfu*, A2 – 0.51–0.66 *apfu*, B1 – 0.95–1.01 *apfu* (Mirošov) and ≤0.04 *apfu* (Pikárec)), Na (A1 – 0.05–0.47 *apfu*, A2 – ≤0.03 *apfu*, B1 – 0.00 *apfu* (Mirošov) and ≤0.25 *apfu* (Pikárec)) and Mg (A1 – ≤0.08 *apfu*, A2 – 0.15–0.43 *apfu*, B1 – 0.26–0.29 *apfu* (Mirošov) and 0.00 *apfu* (Pikárec)). Trace amounts of Ba (A1 – ≤0.08 *apfu*, A2 – 0.04–0.07 *apfu*) and Sr (A1 – 0.02–0.04 *apfu*, A2 – 0.02 *apfu*) were found in chabazite-(Ca) from Věžná I pegmatite whereas traces of Fe occur only in chabazite-(K) from Mirošov (B1 – 0.04–0.05 *apfu*). Chabazite analyses also differ significantly in the Si/Al ratio (A1 – 2.48–2.53, A2 – 2.48–2.54, B1 – 3.14–3.25 (Mirošov) and 2.38–2.50 (Pikárec); Fig. 6a,b).

Minerals of **phillipsite group** with dominant harmotome are common and show the highest compositional variations; however, the number of extra-framework cations is lower comparing the chabazite-group minerals. Several distinct assemblages were recognized (Tab. 3a,b, 5; Fig. 7): (A1) **harmotome** associated with pollucite and chabazite-(Ca), (A2) **harmotome** in cordierite pseudomorph both from the Věžná I pegmatite and **phillipsite-(Ca)** to **harmotome** replacing or overgrowing prehnite from the Věžná II pegmatite, (A3) common **phillipsite-(Ca)** to **harmotome** at fissures from the Věžná II pegmatite and (D) **harmotome** from fissure-filling veinlets in the Rožná–Olší ore field (Tab. 1, 2). The individual types show moderate to very high compositional varia-

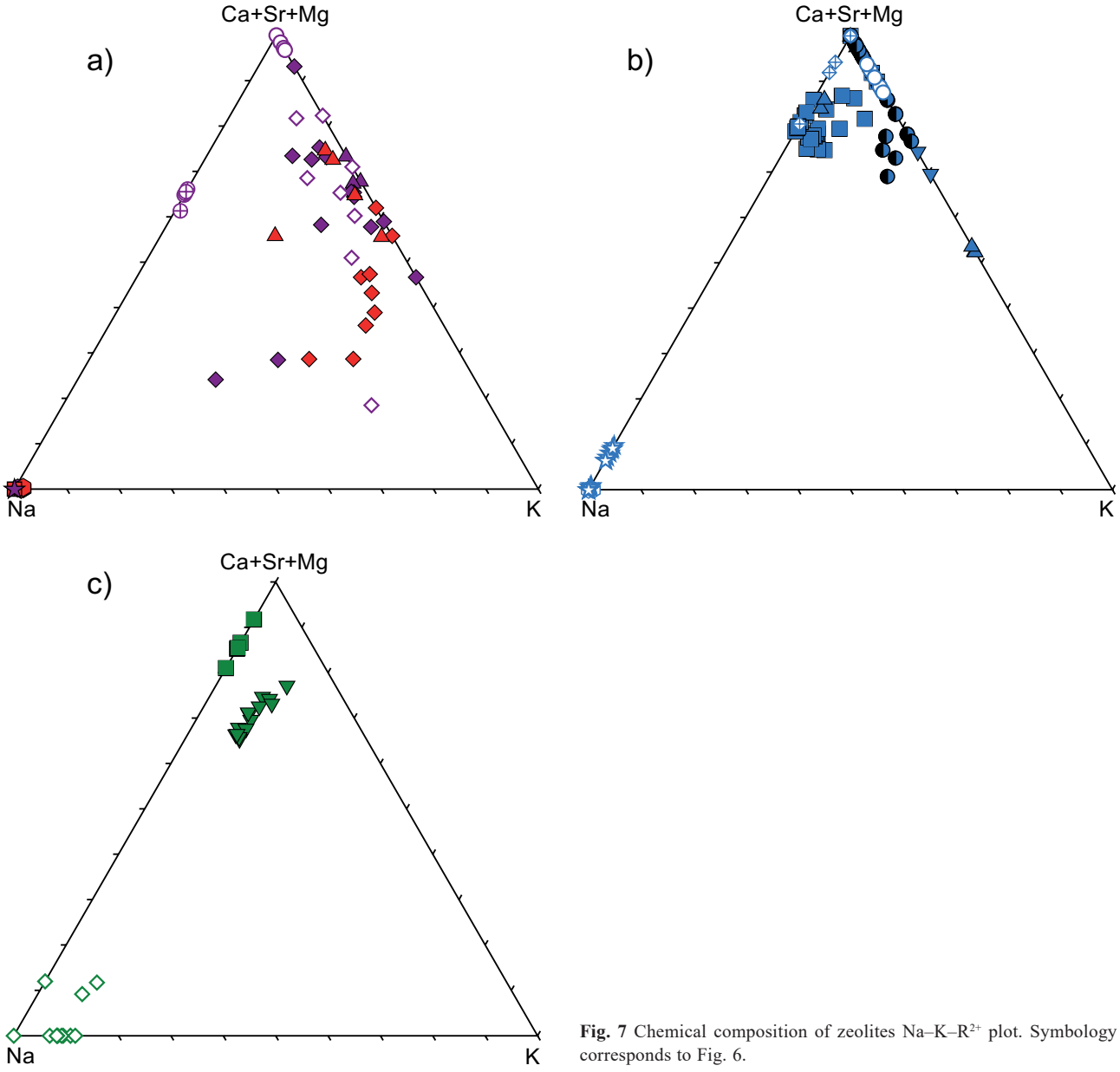

Fig. 7 Chemical composition of zeolites Na–K–R^{2+} plot. Symbology corresponds to Fig. 6.

tions (Fig. 8): Ba (A1 – 1.05–1.82 *apfu*, A2 – 1.80 *apfu* (Věžná I) and 0.09–1.95 *apfu* (Věžná II), A3 – 0.73–1.82 *apfu*, D – 1.88–2.18 *apfu*), K (A1 – 0.26–0.78 *apfu*, A2 – 0.23 *apfu* (Věžná I) and 0.04–1.20 *apfu* (Věžná II), A3 – 0.06–1.07 *apfu*, D – ≤0.10 *apfu*), Ca (A1 – 0.18–0.85 *apfu*, A2 – 0.12 *apfu* (Věžná I) and 0.03–1.79 *apfu* (Věžná II), A3 – 0.00–1.40 *apfu*, D – ≤0.06 *apfu*) and Na (A1 – ≤0.21 *apfu*, A2 – 0.43 *apfu* (Věžná I) and ≤0.19 *apfu* (Věžná II), A3 – ≤0.28 *apfu*, D – 0.00–1.01 *apfu*). Harmotome from the Rožná-Olší ore field is significantly enriched in Na but poor in Ca and K. Minerals of phillipsite group from the individual paragenetic type show mostly high variations in Si/Al ratio (A1 – 2.28–2.45, A2 – 2.56 (Věžná I) and 1.80–3.02 (Věžná II), A3 – 1.76–2.81, D – 2.19–2.58; Fig. 6a,c).

4.4. Chemical composition of zeolites from the individual geological environments

The individual zeolite mineralizations differ significantly in the participation of extra-framework cations. Zeolites from granitic pegmatites (A) are highly variable in the participation of extra-framework cations. The zeolites associated with pollucite (A1) include analcime, chabazite-(Ca) and harmotome. Analcime replacing pollucite is Cs-enriched as in other pegmatite occurrences where it typically replaces pollucite likely as a cation exchange process (e.g., Teertstra et al. 1993, 1995, 1996; Teertstra and Černý 1995, 1997). Chabazite-(Ca) (A1, A2) occur in granitic pegmatites Věžná I (Tab. 3a,b) and contains an elevated number of extra-framework cations chiefly Mg although its concentra-

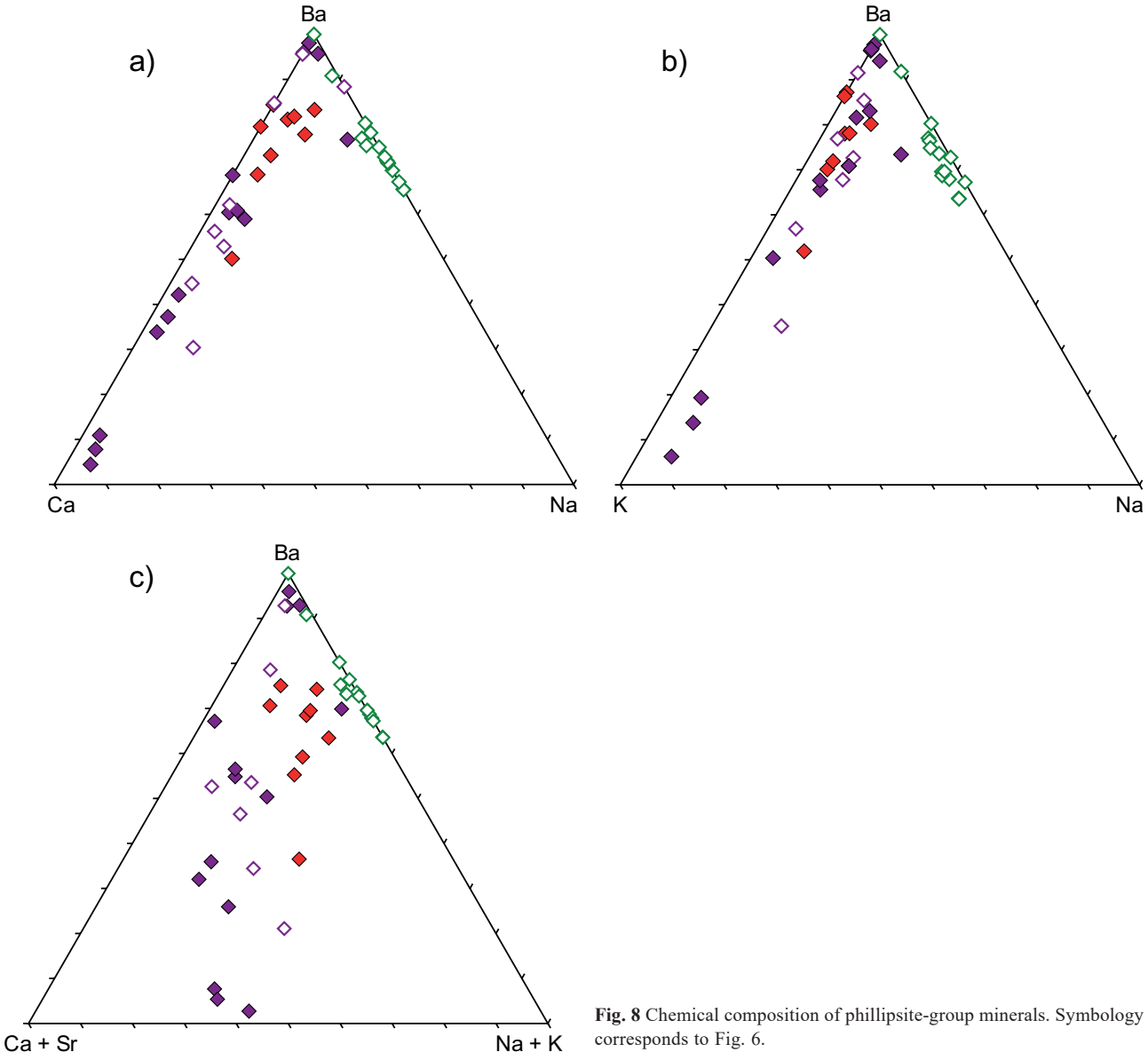

Fig. 8 Chemical composition of phillipsite-group minerals. Symbology corresponds to Fig. 6.

tions are very low in chabazite-(Ca) associated with pollucite (A1) (Mg≤0.08 *apfu*) but high in microscopic veinlets (A2) replacing chabazite-(Ca) in Věžná I (Mg≤0.43 *apfu*). Elevated concentrations of Mg in chabazite-(Ca) from some localities where other zeolites have Mg below the detection limit manifest high compatibility of Mg in chabazite. Minerals of phillipsite group show the highest compositional variations, including harmotome and phillipsite-(Ca); however, they contain a rather low number of other extra-framework cations. Crystals also show zoned texture (Fig. 3f), whereas crystals of other zeolites are compositionally less variable. Phillipsite-group minerals from granitic pegmatites (A1, A2, A3) are compositionally highly variable, mainly in Ba, Ca and K, but always poor in Na. Thomsonite-(Ca) from Věžná II is close to the ideal formula. Laumontite from Domanínek is enriched in K (≤0.133 *apfu*; Tab. 3b).

In the Alpine-type hydrothermal veins (B), which almost exclusively cut amphibolites (ESM 1), Ca-zeolites predominate. Laumontite is compositionally variable (Fig. 9b); in the Alpine-type vein Pikárec (B1) is close to the ideal formula, whereas laumontite from the laumontite (B2) and natrolite veinlets (B3) is evidently K-enriched (Tab. 4a, b). Heulandite-(Ca) from (B1) Alpine-type veins at Mirošov contains several extra-framework cations in elevated concentrations (Fig. 7a,c). Stilbite-(Ca) from the Alpine-type veins in Mirošov (B1) is heterogeneous with highly variable Na and K, whereas stilbite-(Ca) from a similar Alpine-type vein in Pikárec (B1) has K below the detection limit.

Zeolites from the Rožná–Olší ore field occur in two distinct assemblages – stilbite veins from the Jasan Mine, 16th level (C) and harmotome veinlets on brittle fissures (D). Stilbite-(Ca) contains high Na and low K comparing stilbite-

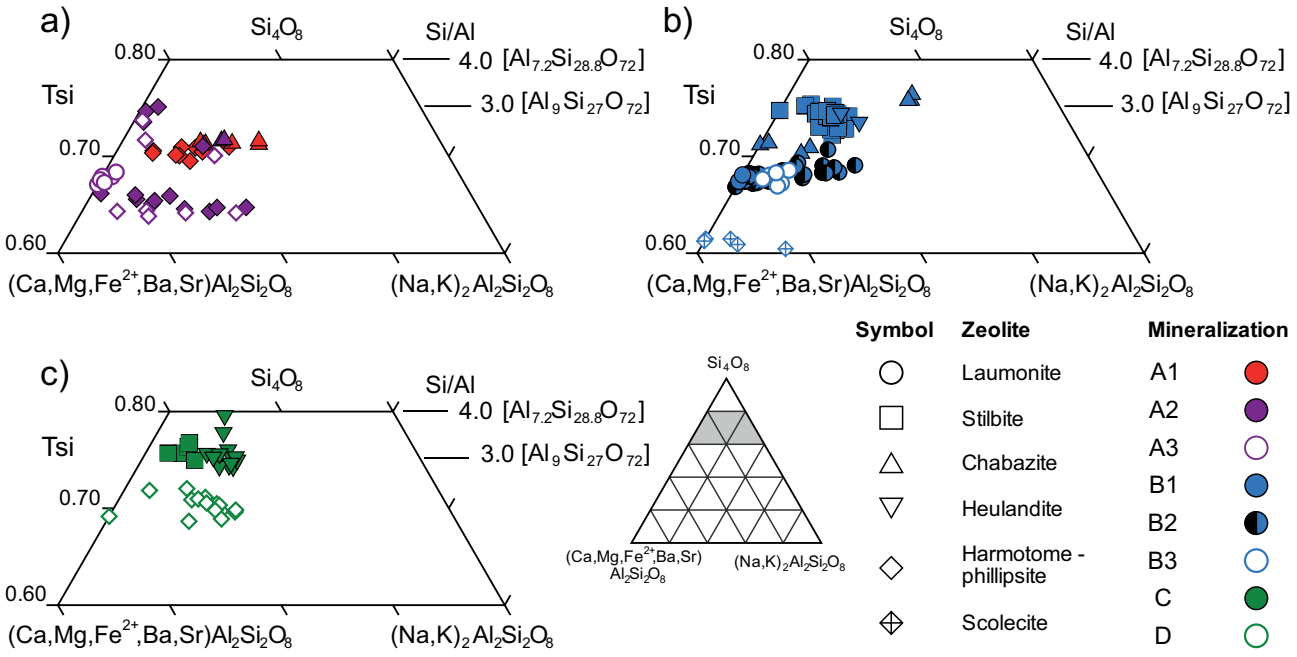

Fig. 9 Diagram Si–R^{2+}AlSi–R^{+}AlSi for the studied zeolites, detail of Fig. 6.

(Ca) from Alpine-type veins (B1). Associated heulandite-(Ca) is always Na-enriched but K-poor (Tab. 5) and contains high concentrations of Mg≤0.48 *apfu* and particularly Sr≤0.90 *apfu* also in heulandite-(Ca) from the Alpine-type vein in Mirošov (B1) with 0.55–0.70 *apfu* Sr (Tab. 4a). Harmotome from veinlets (D) differs from phillipsite-(Ca) to harmotome from granitic pegmatites (A1, A2) in moderate to high contents of Na but very low Ca and K.

The main individual paragenetic types of zeolite mineralizations in the examined region differ in the overall abundances of extra-framework cations (Tab. 6, 7). Primary zeolites (A1) from the Věžná I pegmatite – Cs, Ba, Ca, Na > K > Mg; zeolites from pseudomorphs (A2) – Ca, K > Ba > Na > Mg; fissure-filling zeolites (A3) mainly from the Věžná II pegmatite – Ca, K > Ba > Na; Alpine-type veins with epidote (B1) – Ca > K, Na; laumontite veinlets (B2) – Ca > K > Na; natrolite veinlets (B3) – Na > Ca; stilbite veins (C) – Ca > K, Na and the fissure-filling veinlets with harmotome (D) – Ba >> Na; if we also include common calcite in some harmotome fissures Ba ~ Ca > Na. Comparing the other zeolite mineralizations (A, B) Ca- or Ba-rich zeolites from the Rožná–Olší ore field (C, D) are typically enriched in Na but poor in K.

4.5. Raman spectroscopy

Raman spectroscopy was used mainly to prove the results of EMPA identification of the individual zeolites. We present data (ESM 2, 3) for laumontite, natrolite, scolecite, chabazite, heulandite, harmotome, analcime, and associated prehnite and apophyllite from different mineral assemblages. As the individual zeolites are commonly intimately intergrown or intergrown with other phases, or they occur in minute grains, Raman spectroscopy appears to be a useful tool for the identification of zeolites and associated minerals not only from the rough samples but also from the thin and polished sections. The Raman band positions and relative intensities in the acquired spectral range of the abovementioned minerals are consistent with the published data for these minerals (Adams et al. 1981; Goryainov and Smirnov 2001; Łodziński et al. 2005; Zhang et al. 2018). The spectral match was also confirmed by KnowItAll spectroscopy analytical software (Wiley Science Solutions) in combination with the RRUFF Raman spectra database (Lafuente et al. 2015)

5. Discussion

5.1. Geochemical implications from the chemical composition of zeolites

Chemical compositions of some examined zeolites show high variations or elevated concentrations of extra-framework cations. Bucher and Weisenberger (2013) found that higher concentrations of K in stilbite-(Ca) from Alpine-type veins in the Alps are controlled by meteoritic waters rich in K. Stilbite-(Ca) from the Alpine-type veins (B1) in the Mirošov quarry is K-enriched whereas stilbite-(Ca) from very similar assemblage in drill hole from Pikárec is K-free (Tab. 4a); consequently, this K-enrichment may be

Tab. 4a Representative chemical analyses of zeolites from Alpine-type hydrothermal veins (B1).

Mineralization	B1										
Locality	Mirošov					Pikárec					
Zeolite	Stb-Ca	Stb-Ca	Cbz-K	Hul-Ca	Hul-Ca	Stb-Ca	Stb-Ca	Cbz-Ca	Cbz-Ca	Lmt	Lmt
SiO_2 (wt.%)	56.91	55.71	61.73	57.03	56.79	59.39	56.90	52.19	49.35	52.09	52.54
Al_2O_3	16.62	17.70	16.69	17.47	16.57	17.73	16.32	17.86	17.63	21.42	21.52
CaO	8.18	8.23	5.48	5.56	5.26	8.89	8.40	9.38	9.27	12.40	12.30
BaO	bdl	bdl	bdl	1.27	1.17	bdl	bdl	bdl	bdl	bdl	bdl
SrO	bdl	bdl	bdl	2.59	2.04	bdl	bdl	bdl	bdl	bdl	bdl
FeO	bdl	bdl	0.35	bdl	1.45	bdl	bdl	bdl	bdl	bdl	bdl
MgO	0.07	bdl	1.19	bdl	0.62	bdl	bdl	bdl	bdl	bdl	bdl
K_2O	0.39	0.56	5.11	2.55	2.08	bdl	bdl	bdl	0.18	bdl	bdl
Na_2O	0.43	0.93	bdl	bdl	bdl	1.14	0.93	bdl	0.70	bdl	bdl
Cs_2O	bdl	bdl	bdl	bdl	bdl	bdl	bdl	bdl	bdl	bdl	bdl
P_2O_5	bdl	bdl	bdl	bdl	bdl	bdl	bdl	bdl	bdl	bdl	bdl
F	bdl	bdl	bdl	bdl	bdl	bdl	bdl	bdl	bdl	bdl	bdl
H_2O*	17.40	16.87	9.45	13.53	14.02	12.85	17.45	20.57	22.87	14.09	13.64
∑ oxide	100.00	100.00	100.00	100.00	100.00	100.00	100.00	100.00	100.00	100.00	100.00
Si (*apfu*)	26.849	26.297	9.029	26.586	26.630	26.596	26.876	8.586	8.432	16.116	16.151
Al	9.240	9.846	2.877	9.597	9.158	9.356	9.084	3.464	3.550	7.807	7.797
∑ T	36.089	36.143	11.906	36.183	35.788	35.952	35.960	12.050	11.982	23.923	23.948
Ca	4.081	4.110	0.847	2.743	2.611	4.211	4.196	1.632	1.676	4.059	4.001
Ba	—	—	—	0.231	0.215	—	—	—	—	—	—
Sr	—	—	—	0.700	0.554	—	—	—	—	—	—
Fe	—	—	0.043	—	0.570	—	—	—	—	—	—
Mg	0.049	—	0.259	—	0.431	—	—	—	—	—	—
K	0.235	0.206	0.953	1.517	1.244	—	—	—	0.038	—	—
Na	0.393	0.851	—	—	—	0.989	0.853	—	0.232	—	—
Cs	—	—	—	—	—	—	—	—	—	—	—
P	—	—	—	—	—	—	—	—	—	—	—
F	—	—	—	—	—	—	—	—	—	—	—
∑ cat	4.758	5.167	2.102	5.191	5.625	5.200	5.049	1.632	1.946	4.059	4.001
H_2O	27.403	26.582	4.614	21.056	21.947	19.209	27.515	11.297	13.046	14.553	13.999
Si/Al	2.91	2.67	3.14	2.77	2.91	2.84	2.96	2.48	2.38	2.06	2.07
T_{Si}	0.74	0.73	0.76	0.73	0.74	0.74	0.75	0.71	0.70	0.67	0.67
E%	3.94	6.14	–9.15	8.23	3.39	–0.53	–1.84	6.14	–2.20	–3.82	–2.50

Note: *H_2O calculated by difference; bdl = below detection limit

caused by meteoritic water. Elevated concentrations of Sr were found especially in heulandite-(Ca) from different mineral assemblages (Tab. 4a, 5). They were likely facilitated by the crystal-structural constraints because Sr-enriched heulandite was found in the Alpine-type veins associated with other Sr-free or Sr-poor Ca-zeolites (Weisenberger and Bucher 2010). Hence, heulandite-(Ca) behaves as a sink of Sr along with chabazite and thomsonite; however, concentrations of Sr are significantly lower (Tab. 3, 4, 5).

The aqueous activity of Si in hydrothermal fluids is indicated by Si/Al ratio in zeolites (see Fig. 9) and the occurrence of quartz in the zeolite assemblages with silica-oversaturated [heulandite-(Ca), stilbite-(Ca), laumontite] to silica-undersaturated [natrolite, analcime, thomsonite-(Ca)] assemblages. Quartz is present only at the Alpine-type veins (B1) from Mirošov. It is the earliest mineral in the assemblages and is overgrown by stilbite-(Ca) (Fig. 4a). The analcime samples from kerolite pseudomorphs at the Věžná I pegmatite have slightly variable Si/Al ratio (2.06–2.13) (Fig. 9a, Tab. 3b). Heulandite-(Ca) shows significant variations in Si/Al ratio (2.77–3.89, Fig. 9b, c) as well as the chabazite samples (2.48–3.14). Minerals of the phillipsite group from the individual paragenetic type show the highest variations within the individual samples (1.80–3.02 in zoned phillipsite-(Ca)-harmotome from Věžná II; Fig. 9a, c). The variations in Si/Al ratio of the individual minerals or mineral groups/series are consistent with the data of Chipera and Apps (2001) and the highest variations reflect the zoning of the individual crystals (Fig. 3f).

Crystallization sequences of zeolites were only scarcely observed because a single zeolite is mostly present in tectonic fractures and fissures. The observed sequences from the Alpine-type hydrothermal veins (B1): laumontite → stilbite-(Ca), and from stilbite veins (C): stilbite-(Ca) → chabazite-(Ca), and heulandite-

Tab. 4b Representative chemical analyses of zeolites from Alpine-type hydrothermal veins (B2, B3).

Mineralization	B2								B3								
Locality	Moravec		Mostiště		Velké Meziříčí		Nové Veselí		Mirošov		Mostiště			Nové Veselí			
Zeolite	Lmt	Lmt	Lmt	Lmt	Lmt	Lmt	Lmt	Lmt	Ntr	Ntr	Ntr	Ntr	Slc	Ntr	Ntr	Anl	Lmt
SiO_2 (wt.%)	53.22	52.60	51.68	53.26	51.84	52.57	50.99	50.21	47.69	47.79	47.82	48.77	45.87	48.58	47.75	56.05	50.96
Al_2O_3	21.09	21.05	20.52	21.33	19.69	20.18	20.45	20.58	26.75	26.79	26.09	25.41	24.98	25.13	25.65	21.89	21.36
CaO	11.83	11.58	11.79	12.68	9.34	9.92	11.68	11.82	0.28	bdl	0.15	2.42	13.96	bdl	bdl	bdl	11.76
BaO	bdl	bdl	bdl	bdl	bdl	bdl	bdl	bdl	bdl	bdl	bdl	bdl	bdl	bdl	bdl	bdl	bdl
SrO	bdl	bdl	bdl	bdl	bdl	bdl	bdl	bdl	bdl	bdl	bdl	bdl	bdl	bdl	bdl	bdl	bdl
FeO	bdl	bdl	bdl	bdl	bdl	bdl	bdl	bdl	bdl	bdl	bdl	bdl	bdl	bdl	bdl	bdl	bdl
MgO	bdl	bdl	bdl	bdl	bdl	bdl	bdl	bdl	bdl	bdl	bdl	bdl	bdl	bdl	bdl	bdl	bdl
K_2O	0.40	0.86	0.21	0.33	2.53	2.06	0.21	bdl	bdl	bdl	bdl	bdl	bdl	bdl	bdl	0.18	1.23
Na_2O	bdl	bdl	bdl	bdl	0.62	0.46	bdl	bdl	15.43	15.80	15.24	12.21	0.67	15.72	15.12	13.66	bdl
Cs_2O	bdl	bdl	bdl	bdl	bdl	bdl	bdl	bdl	bdl	bdl	bdl	bdl	bdl	bdl	bdl	bdl	bdl
P_2O_5	bdl	bdl	bdl	bdl	bdl	bdl	bdl	bdl	bdl	bdl	bdl	bdl	bdl	bdl	bdl	bdl	bdl
F	bdl	bdl	bdl	bdl	bdl	bdl	bdl	bdl	bdl	bdl	bdl	bdl	bdl	bdl	bdl	bdl	bdl
H_2O*	13.46	13.91	15.80	12.40	15.98	14.81	16.67	17.39	9.85	9.62	10.70	11.19	14.52	10.57	11.48	8.22	14.69
∑ oxide	100.00	100.00	100.00	100.00	100.00	100.00	100.00	100.00	100.00	100.00	100.00	100.00	100.00	100.00	100.00	100.00	100.00
Si (*apfu*)	16.322	16.267	16.294	16.195	16.510	16.349	16.248	16.141	3.020	3.020	3.052	3.109	3.031	3.098	3.070	2.049	15.998
Al	7.626	7.673	7.624	7.645	7.389	7.396	7.681	7.798	1.997	1.995	1.962	1.909	1.946	1.889	1.944	0.943	7.902
∑ T	23.948	23.940	23.918	23.840	23.899	23.745	23.929	23.939	5.017	5.015	5.014	5.018	4.977	4.987	5.014	2.992	23.900
Ca	3.839	3.788	3.933	4.078	3.148	3.263	3.939	4.020	0.018	—	0.010	0.163	0.976	—	—	—	3.904
Ba	—	—	—	—	—	—	—	—	—	—	—	—	—	—	—	—	—
Sr	—	—	—	—	—	—	—	—	—	—	—	—	—	—	—	—	—
Fe	—	—	—	—	—	—	—	—	—	—	—	—	—	—	—	—	—
Mg	—	—	—	—	—	—	—	—	—	—	—	—	—	—	—	—	—
K	0.155	0.339	0.084	0.128	1.030	0.818	0.086	—	—	—	—	—	—	—	—	0.008	0.493
Na	—	—	—	—	0.390	0.279	—	—	1.894	1.936	1.886	1.509	0.086	1.943	1.885	0.968	—
Cs	—	—	—	—	—	—	—	—	—	—	—	—	—	—	—	—	—
P	—	—	—	—	—	—	—	—	—	—	—	—	—	—	—	—	—
F	—	—	—	—	—	—	—	—	—	—	—	—	—	—	—	—	—
∑ cat	3.994	4.127	4.017	4.206	4.568	4.360	4.025	4.020	1.912	1.936	1.896	1.672	1.062	1.943	1.885	0.976	4.397
H_2O	13.782	14.361	16.631	12.587	16.989	15.375	17.734	18.665	2.082	2.029	2.280	2.381	3.203	2.250	2.464	1.003	15.396
Si/Al	2.14	2.12	2.14	2.12	2.23	2.21	2.12	2.07	1.51	1.51	1.56	1.63	1.56	1.64	1.58	2.17	2.02
T_{Si}	0.68	0.68	0.68	0.68	0.69	0.69	0.68	0.67	0.60	0.60	0.61	0.62	0.61	0.62	0.61	0.68	0.67
E%	–2.68	–3.16	–4.03	–7.72	–4.28	–2.89	–3.64	–2.99	3.63	3.09	3.70	4.37	–4.89	–2.58	4.30	2.65	–4.70

Note: *H_2O calculated by difference; bdl = below detection limit

(Ca) → stilbite-(Ca) → chabazite-(Ca) suggest decreasing T and perhaps P (Fig. 1a, b) but also decreasing of $aSiO_2$ during crystallization (Fig. 1b). Low $aSiO_2$ under the quartz saturation is manifested by the absence of quartz in all zeolite assemblages except for the Alpine-type veins (C1) from Mirošov (Tab. 2).

The absence of carbonates in most zeolite assemblages except for harmotome veinlets (D) is a typical feature. It suggests low aCO_2 in these assemblages and confirms that low aCO_2 is required for the origin/crystallization of zeolites, particularly in low T (Weisenberger and Bucher 2010). Solely harmotome veinlets (D) from U-mines in the Rožná-Olší ore field contain locally abundant cogenetic calcite (Fig. 5c, d) and it indicates mineralized fluids enriched in CO_2 solely in this zeolite assemblage.

5.2. Estimation of PTX conditions of the selected zeolite assemblages from tectonic fractures and fissures

We made an attempt to estimate PTX conditions for the selected Ca-rich paragenetic types of zeolite mineralizations developed on tectonic fractures and fissures (A3, B1, B2, B3, C, D). The zeolite assemblages from the pegmatites (A1, A2) were only briefly mentioned and not given in Fig. 10. Nevertheless, the estimations were complicated due to several factors: wide stability fields of most zeolites (Fig. 1) and some associated minerals (e.g., Frey and Robinson 2009; Weisenberger 2009); compositional variability in some zeolites Ca, K- or Ba-dominant species (phillipsite group, chabazite group); a large number of factors controlling the stability of zeolites (e.g., Chipera and Apps 2001; Williams and Carr 2005; Weisenberger 2009). Because the mineral assemblages and sequences of crystallization in the examined Alpine-type fractures and fissures are quite similar to the Alpine-type hydrothermal veins from the Central Alps (Weisenberger 2009) we applied the retrograde PT-path elucidated from fluid inclusions in fissure quartz in this region (Fig. 1a; Mullis et al. 1994) in our discussion.

5.2.1. Granitic pegmatites

(A1) In the pegmatite Věžná I, early pollucite I sequestered at T > 350 °C (very likely T < 400 °C), followed by the subsolidus analcimization of pollucite I at T < ~150–200 °C (Teertstra and Černý 1995; London et al. 1998; London 2008, 2018; Toman and Novák 2018). Emplacement of pegmatite melts at P < ~200–300 MPa (lithostatic pressure) is assumed for the rare-element granitic pegmatites of the Moldanubian Zone (Ackermann et al. 2007; Novák et al. 2013, 2015a). (A2) The temperatures estimated for the zeolite assemblage (analcime + natrolite) from the pseudomorphs after quartz with dominant kerolite (Věžná I; Dosbaba and Novák 2012) and for natrolite after tourmaline obtained from the associated chlorite thermometry (Drahonín VI; Čopjaková et al. 2021) are T < ~100–300 °C and T < ~170–200 °C, respectively. (A3) Fissure-filling zeolite assemblages from granitic pegmatites (thomsonite, phillipsite-(Ca) to harmotome), followed alteration of feldspars and origin of prehnite stable at T > ~200–250 °C (Frey and Robinson 2009; Weisenberger 2009); consequently, low T < ~150 °C for the crystallization of these zeolites is feasible. Cha-

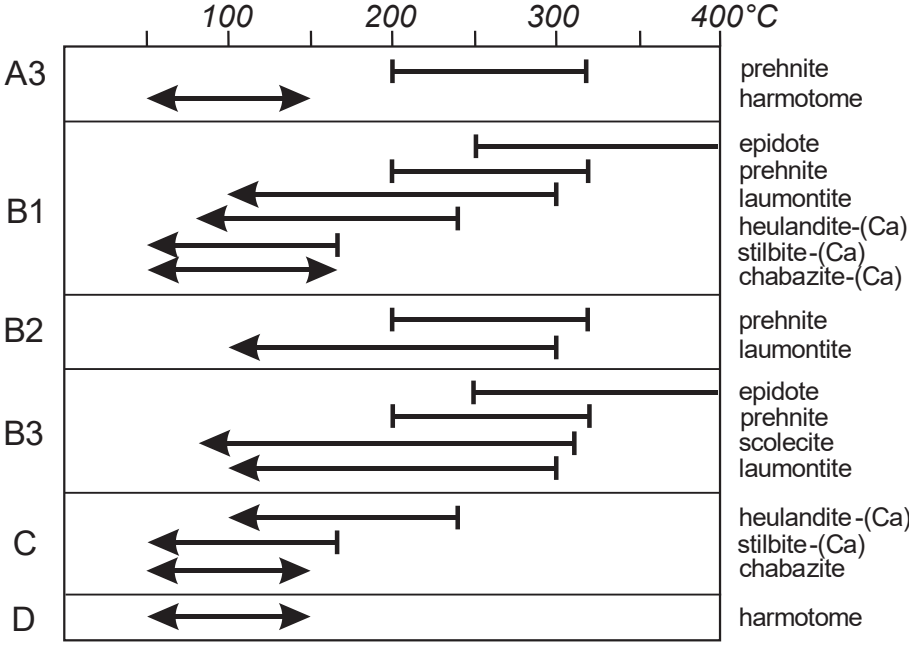

Fig. 10 Thermal ranges of minerals from the selected fracture-filling zeolite mineralizations. Their estimations are based on the published stability fields for individual minerals. The upper limits are based on experimental and thermodynamic data (Perrotta 1976; Frey and Robinson 2009; Weisenberger and Bucher 2010), whereas the lower limits in zeolites marked by arrows were estimated from thermodynamic modeling (Chipera and Apps 2001) and empirical data on crystallization sequences from zeolite mineralizations in volcanic regions (Apps 1983; Iijima 2001; Karlsson 2001; Utada 2001a; Weisenberger and Selbekk 2009). Arrows in the upper limit are given in harmotome and chabazite-(Ca) with high content of K due to the absence of experimental data. Real temperatures of most zeolite crystallizations are likely be close to the low-T limits at about 150 to 50 °C.

Tab. 5 Representative chemical analyses of zeolites from the Rožná-Olší ore field (C, D).

Mineralization	C						D		
Locality	Dolní Rožínka-Jasan mine – 16th level						Dolní Rožínka		
Zeolite	Stb-Ca	Stb-Ca	Stb-Ca	Hul-Ca	Hul-Ca	Hul-Ca	Hrm	Hrm	Hrm
SiO_2 (wt.%)	58.02	56.53	59.41	57.09	57.95	58.50	51.49	51.17	51.52
Al_2O_3	16.43	15.38	15.24	16.76	16.15	16.60	18.96	18.78	18.31
CaO	8.46	8.29	8.45	5.69	5.04	5.51	bdl	bdl	bdl
BaO	bdl	bdl	bdl	0.49	0.71	0.52	22.45	22.46	23.23
SrO	bdl	bdl	bdl	3.19	2.99	3.16	bdl	bdl	bdl
FeO	bdl	bdl	bdl	bdl	bdl	bdl	bdl	bdl	bdl
MgO	bdl	bdl	bdl	bdl	bdl	bdl	bdl	bdl	bdl
K_2O	bdl	bdl	bdl	0.80	0.86	0.97	0.27	0.28	0.34
Na_2O	1.08	0.41	0.79	1.12	1.34	1.47	1.97	1.80	1.83
Cs_2O	bdl	bdl	bdl	bdl	bdl	bdl	bdl	bdl	bdl
P_2O_5	bdl	bdl	bdl	bdl	bdl	bdl	bdl	bdl	bdl
F	bdl	bdl	bdl	bdl	bdl	0.12	bdl	bdl	bdl
H_2O*	16.01	19.39	16.11	14.86	14.96	13.15	4.86	5.51	4.77
∑ oxide	100.00	100.00	100.00	100.00	100.00	100.00	100.00	100.00	100.00
Si (*apfu*)	26.935	27.241	27.516	26.781	27.160	26.891	11.179	11.194	11.252
Al	8.992	8.736	8.318	9.270	8.920	8.997	4.853	4.843	4.715
∑ T	35.927	35.977	35.834	36.051	36.080	35.888	16.032	16.037	15.967
Ca	4.155	4.224	4.139	2.824	2.497	2.679	—	—	—
Ba	—	—	—	0.091	0.130	0.093	1.910	1.926	1.988
Sr	—	—	—	0.867	0.813	0.842	—	—	—
Fe	—	—	—	—	—	—	—	—	—
Mg	—	—	—	—	—	—	—	—	—
K	—	—	—	0.479	0.515	0.567	0.076	0.077	0.094
Na	0.974	0.381	0.706	1.022	1.218	1.312	0.828	0.764	0.775
Cs	—	—	—	—	—	—	—	—	—
P	—	—	—	—	—	—	—	—	—
F	—	—	—	—	—	0.170	—	—	—
∑ cat	5.129	4.605	4.845	5.283	5.173	5.663	2.814	2.767	2.857
H_2O	24.813	31.192	24.907	23.272	23.403	20.180	3.523	4.024	3.478
Si/Al	3.00	3.12	3.31	2.89	3.04	2.99	2.30	2.31	2.39
T_{Si}	0.75	0.76	0.77	0.74	0.75	0.75	0.70	0.70	0.72
E%	–3.23	–0.91	–7.35	2.32	3.48	–1.10	2.75	2.99	–2.28

Note: *H_2O calculated by difference; bdl = below detection limit

bazite-(Ca) and harmotome are rather low-T zeolites and their crystallizations at T<~100–150 °C and P<~50 MPa are very likely (Fig. 10).

5.2.2. Alpine-type hydrothermal veins

(B1) The temperature range of ~250–400 °C is feasible for the crystallization of early minerals – epidote and prehnite (e.g., Liou et al. 1983, 1985; Frey and Robinson 2009; Weisenberger and Bucher 2010, 2011) in the Alpine-type hydrothermal veins at Mirošov and Pikárec (Fig. 10). The pressure P<~100–200 MPa was estimated for early assemblage epidote+prehnite from the analogical Alpine-type veins in the Central Alps (Fig. 1a; Mullis et al. 1994) and supported by ductile to brittle character of host tectonic fractures. Zeolites in open vugs (e.g., laumontite) overgrowing epidote and/or prehnite crystallized below the low-T limit for epidote and prehnite (T~200–250 °C; Frey and Robinson 2009) at T<~150–200 °C (e.g., Weisenberger 2009; Weisenberger and Bucher 2010) and late zeolites [stilbite-(Ca), chabazite-(Ca), chabazite-(K)] at lower T. The pressure for the zeolite crystallization is approximated from the data of Mullis et al. (1994) at P<~50 MPa (hydrostatic pressure). Thin laumontite (B2) and natrolite (B3) veinlets with rare early prehnite and epidote may have started to crystallize at T~250–400 °C, similar to the Alpine-type hydrothermal veins (B1). However, due to scarcity of early minerals (epidote, prehnite), the brittle character of fissures, and lower degree of alteration of host rocks relative to the assemblage (B1), the zeolite crystallization started about the lower T limit of epidote and prehnite at T~200–250 °C or even less (Fig. 10). This process did not facilitate origin of open vugs and radial aggregates of laumontite and natrolite at some fissures suggest no preferential orientation during their grow. Additionally,

the occurrence of scolecite at the (B3) natrolite veinlets from Mostiště indicates low P<~15 MPa (Weisenberger 2009) in this assemblage. The upper temperatures elucidated for the Alpine-type hydrothermal veins (B1) and laumontite (B2) and natrolite (B3) veinlets at T~250 °C discussed above are very similar to the T=~250–300 °C presented for the retrograde stage of Variscan metamorphism from the fluid inclusion study at the Rožná–Olší ore field by Kříbek et al. (2009).

5.2.3. Hydrothermal veins in the Rožná–Olší ore field

(C) The stilbite veins with abundant zeolites and common pyrite from the Jasan Mine, 16th level generally crystallized at lower T relative to the Alpine-type veins (B1) which are characterized by common early high-T minerals – epidote and prehnite (Fig. 10). Nevertheless, strong alteration of host rocks and ductile to the brittle character of stilbite veins suggest that the crystallization of early zeolite – heulandite-(Ca) was likely closer to its upper limit at T<~240 °C (Fig. 10). It is in contrast with the (D) harmotome fissure-filling veinlets spatially related to U-mineralizations. They are characterized by an almost total absence of alteration of the host rock in all samples, brittle behavior and variability of host rocks. Harmotome is stable at low T estimated from its relation to other zeolites in the crystallization sequences and experimental data (Perrotta 1976). Crystallization of the fissure-filling harmotome (D) at T~50–100 °C is very likely. The pressure was estimated at P<~50 MPa for the stilbite veins (C) and very likely at lower P~10–30 MPa for the harmotome veinlets (D). The formation of harmotome veinlets is a low-T process comparable with the fissure-filling harmotome assemblage in granitic pegmatite fissures (A3). Also, Kříbek et al. (2009) considered zeolites the latest minerals at the Rožná U-deposit.

5.3. Sources of cations for the individual textural and paragenetic types of zeolite mineralizations

The individual textural and paragenetic types of zeolite mineralizations differ significantly in relation to overall geological evolution from early granitic pegmatites (A), retrograde metamorphic assemblages of the Alpine-type hydrothermal veins (B) to a variety of hydrothermal assemblages (C, D) very likely related to the pre-uranium quartz-sulfide and carbonate-sulfide mineralizations, uranium mineralization and post-uranium carbonate-quartz-sulfide mineralizations recognized at the Rožná-Olší ore field by Kříbek et al. (2009).

5.3.1. Granitic pegmatites

(A1) Nodular aggregates of zeolites from late magmatic to early hydrothermal stage in the Věžná I pegmatite (Tab. 1, 2) with the dominant cations Cs, Ba, Ca, K, and Na (Tab. 6, 7) have geochemical signature entirely different from all other types of zeolite mineralizations examined in this region; pegmatite melt was the source of all relevant cations. Moreover, this complex assemblage differs from all known pollucite occurrences (e.g., Teertstra et al. 1993, 1995, 1996; Teertstra and Černý 1995, 1997) chiefly in high Ba. The absence of Mg except for late veinlets of Mg-enriched chabazite-(Ca) replacing early chabazite-(Ca) (Fig. 3c) suggests crystallization in the system closed to the host rock. Pegmatite melt and residual fluids were sources of cations.

Zeolites, as alteration products of primary minerals (A2) and in fissure-fillings (A3) from all granitic pegmatites (Tab. 1, 2), are compositionally quite variable, although Ca is dominant along with less common Ba, Na, minor K, and traces of Mg (Tab. 6, 7). Occurrences of harmotome in pseudomorphs after cordierite at the Věžná I (Gadas et al. 2020) and rims of harmotome around phillipsite-(Ca) on fissures at the Věžná II pegmatite (Fig. 3f) indicate high activity of Ba typical for the primary zeolite assemblage at the Věžná I pegmatite (Toman and Novák 2018, 2020). However, harmotome was found in other altered primitive pegmatites cutting serpentinite from the Moldanubian Zone (e.g., Hrubšice near Oslavany; Černý and Povondra 1965); consequently, the source of Ba in fluids in the assemblages (A2) and (A3) may be host serpentinite or altered primary feldspars from the host pegmatite; elevated contents of Ba were found in feldspars from the Věžná I pegmatite (Černý et al. 1984). Calcium, Na, and K were sourced from parental pegmatite but part of Ca from host serpentinite as well (Palandri and Reed 2004; Evans et al. 2013; Novák et al. 2017). The processes producing secondary zeolite

Tab. 6 Abundances of the zeolite species in the individual zeolite mineralizations; C – common, M – minor, R – rare.

		A1	A2	A3	A	B1	B2	B3	B	C	D	C+D
pollucite	**Cs**	C			**Cs**							
analcime	**Na**	C	R		**Na**			R				
chabazite-(K)	**K**					R						
chabazite-(Ca)	**Ca**	C	R		**Ca**	R						
harmotome	**Ba**	C	R	M	**Ba**						C	**Ba**
phillipsite-(Ca)	**Ca**		R	C	**Ca**							
thomsonite-(Ca)	**Ca**			C	**Ca**							
natrolite	**Na**		R	R				C	**Na**			
laumontite	**Ca**			R		R	C	C	**Ca**			
stilbite-(Ca)	**Ca**					C			**Ca**	C		**Ca**
heulandite-(Ca)	**Ca**					R				C		**Ca**
scolecite	**Ca**							R				

Tab. 7 Geochemical signature of the individual zeolite mineralizations, including the associated minerals (**A1** – lepidolite, elbaite; **A3, D** – calcite; **B1** – axinite; **C** – pyrite).

Textural/paragenetic type	locality/dominant zeolite at several localities	F	B	S	CO_2	Li	Cs	K	Ca	Na	Ba	Sr	Mg
A1	Věžná I	M	R			R	C	R	C	C	C		
A2	Věžná I, Věžná II, Drahonín VI								C	C	R		R
A3	Věžná II, Domanínek				R			R	C	M	M		M
B1	Mirošov		C					M	C	R		R	R
	Pikárec								C				
B2	laumontite/10 localities							M	C	R			
B3	natrolite/3 localities								M	C			
C	Dolní Rožínka-Jasan 16th level	R		C				M	C			R	
D	Dolní Rožínka, Bukov				M				M	R	C		

C – common, M – minor, R – rare.

assemblages in pseudomorphs (A2) and on fissures (A3) were mostly facilitated by external fluids derived from host serpentinite (Dosbaba and Novák 2012; Novák et al. 2017; Toman and Novák 2018; Čopjaková et al. 2021) after equilibration of the pegmatite and its host rock (Palinkaš et al. 2014) also manifested by elevated concentrations of Mg mainly in late veinlets of chabazite-(Ca) (Fig. 3c, Tab. 3b).

5.3.2. Alpine-type hydrothermal veins

(B1) The Alpine-type hydrothermal veins with epidote + prehnite contain minor, mostly Ca-rich zeolites [Mirošov, Pikárec; laumontite, stilbite-(Ca), chabazite-(Ca), chabazite-(K) and heulandite-(Ca)]. Their compositions reflect strong alteration of the host rock (amphibolite) at comparatively high T and ductile to the brittle character of host rocks during the formation of these mineralized veins is typical. The hydrothermal fluids were generated during retrograde stages of the Variscan metamorphism of host rock complexes. Boron in axinite was likely derived from the host metabasite (Leeman and Sisson 1996) and no additional sources of fluids are feasible.

Thin fissure-filling laumontite (B2) and rare natrolite (B3) veinlets show a rather weak alteration of host rocks and the absence of open vugs. These fluids were generated during retrograde stages of metamorphism at different tectonic conditions and lower availability of fluids comparing the Alpine-type hydrothermal veins (B1) and at lower T (Fig. 10) and P. It is also supported by the brittle behavior of host rocks and the low degree of their alteration. The zeolite assemblages (B1, B2, B3) were evidently facilitated by metamorphic fluids during various retrograde stages of the Variscan metamorphism, e.g., by albitization of plagioclase. They sourced all cations released from host rocks, including Ca and K + Na in the (B2) laumontite veins and Na + Ca in natrolite, analcime, laumontite and scolecite from the (B3) natrolite veins (Tab. 6, 7). However, his process was not studied in detail. Why the laumontite (B2) and natrolite (B3) veinlets occur in the same amphibolite bodies (Fig. 2; ESM 1) is not clear.

5.3.3. Hydrothermal veins in the Rožná–Olší ore field

(C) The stilbite veins (Jasan Mine, 16th level; Šťáva 1981) exhibit high Ca with low K but elevated Na comparing the Alpine-type hydrothermal veins (B1). This assemblage is different from the other zeolite assemblages in the Rožná–Olší ore field by a strong alteration of host rock (calc-silicate rock > amphibolite, marble), rich zeolite assemblage, rare early apophyllite, the abundance of pyrite and presence of other rare sulfides (mainly chalcopyrite and pyrrhotite), and primarily by the transitional ductile to the brittle character of mineralized tectonic fractures. Hydrothermal fluids which supplied relevant cations Ca, K, and Na were enriched in S + Fe + F (± Cu, Ni) and are rather different from the Alpine-type hydrothermal veins (B1) where sulfides are absent as well as F-bearing minerals (apophyllite). Their occurrence solely within the Rožná–Olší ore field suggests their spatial and/or genetic relation to the pre-uranium quartz–sulfide and carbonate–sulfide mineralizations (Kříbek et al. 2009), although mixing with retrograde metamorphic hydrothermal fluids also is possible.

(D) Harmotome veinlets in brittle fissures from the Rožná U-deposit mostly contain only a single zeolite mineral – harmotome, and almost no sulfides and locally common calcite (Tab. 2). They cut various rocks, show open vugs, weak to no alteration of host rocks (Fig. 5c, d) and evident spatial relations to U-mineralization zones and veins. They are assumed to be later then U-mineralization (Kříbek et al. 2009). Calcite locally associated with harmotome at some fissure-filling veinlets demonstrates elevated Ca and CO_2 in hydrothermal fluids along with dominant Ba and minor Na. Very low concentrations of K in harmotome are typical (Tab. 5). Close spatial relations to U-mineralizations suggest that they were generally related to the ore processes, mainly the

post-uranium stage defined by Kříbek and Hájek (2005) and Kříbek et al. (2009).

6. Conclusions and summary

Geological position, textural development, and mineralogy of the individual zeolite mineralizations were a basis for the discussion of their temporal and mutual relations to the retrograde stages of the Variscan metamorphism and to the subsequent post-Variscan processes related to U-mineralization in the Rožná–Olší ore field within the Strážek Unit.

Primary zeolites (A1), mainly pollucite (± chabazite-(Ca) and harmotome) from the pegmatite Věžná I (Toman and Novák 2018) crystallized at T < ~350–400 °C and P < ~200 MPa (lithostatic pressure) equal to the host rock close to the age 336–334 Ma dated in magmatic monazite from the Věžná II pegmatite (Novák et al. 1998). Zeolites as alteration products of primary minerals (A2) or as fissure-filling veinlets (A3) (Tab. 1, 2) are compositionally variable. Both originated during subsolidus stage of pegmatite evolution, mostly related to external fluids likely associated with low-T stages of retrograde metamorphism at a hydrostatic pressure of P < ~50 MPa and T ~50–150 °C.

The distribution of the Alpine-type hydrothermal veins with epidote + prehnite (B1), as well as abundant laumontite (B2) and rare natrolite (B3) veinlets within the Strážek Unit suggest that their origins were evidently facilitated by hydrothermal fluids related to retrograde metamorphism. However, they differ in transitional ductile to the brittle character of mineralized fractures in the Alpine-type hydrothermal veins (B1) and evident brittle character of the fissure-filling veinlets (B2, B3) with laumontite and/or natrolite. Their origins were evidently facilitated by hydrothermal fluids released from their host rocks during retrograde stages of the Variscan metamorphism. The estimated temperatures varied from T ~250–400 °C for early minerals at the Alpine-type veins (B1) at lithostatic pressure P < ~150–200 MPa to T < ~250 °C and hydrostatic pressure P < ~50 MPa for the laumontite (B2) and natrolite (B3) veinlets. These values are similar to the data obtained for the retrograde stage of Variscan metamorphism by Kříbek et al. (2009).

Hydrothermal zeolite veins occurring exclusively at the Rožná–Olší ore field and represented by the stilbite veins (C) with transitional ductile to the brittle character of fractures and the harmotome veinlets (D) on brittle fissures are evidently spatially related the Rožná-Olší ore field. The stilbite veins originated due to the strong alteration of host rock close to the upper T-limit of early heulandite-(Ca) at T < ~240 °C. The fissure-filling veinlets with dominant harmotome (D) cut locally U-mineralization and differ from the stilbite veins (C) in high Ba contents, presence of CO_2-bearing fluids, and absence of host rock alterations. This latest zeolite mineralization (D) is related to the post-U-mineralization processes at low T ~50–100 °C (Fig. 10) and low P < ~20 MPa. The distinct chemical composition of zeolites and associated minerals in both types suggest that the stilbite veins (C) and harmotome veinlets (D) have distinct sources of fluids – host heterogeneous calc-silicate rock and external sources likely related to U-mineralizations, respectively.

The zeolite mineralizations are typically associated with major regional faults, mainly longitudinal N–S to NNW–SSE-striking ductile shear zones Rožná and Olší parallel to the tectonic contact between the Strážek Unit and the Svratka Crystalline Complex (Fig. 2). Zeolites may serve as a suitable indicator of low-T alkaline to neutral hydrothermal conditions with a low aCO_2; they typically mark the latest stage of the individual hydrothermal events. Also, transitional ductile to brittle to evidently brittle fractures with zeolite mineralizations exhibit that their origin is related to distinct tectonic stages of the geological evolution of the host rock complex, including fault/fracture network, which may be related to earthquakes. The examined zeolite mineralizations demonstrate that repeating PTX conditions suitable for the origin of zeolites were achieved in terminations of the independent geological events.

Acknowledgments. The authors thank an anonymous reviewer and B. Kříbek for constructive criticism that significantly improved the manuscript and V. Wertich for technical assistance. This research was supported by OP RDE [grant number CZ.02.1.01/0.0/0.0/16_026/0008459 (Geobarr) from the ERDF] for MN and RŠ. This work also appears through the institutional support of long-term conceptual development of research institutions provided by the Ministry of Culture (ref. MK000094862) for JT.

Electronic supplementary material. ESM is available online at the Journal website (*http://dx.doi.org/10.3190/jgeosci.370*).

References

Ackerman L, Zachariáš J, Pudilová M (2007) P–T and fluid evolution of barren and lithium pegmatites from Vlastějovice, Bohemian Massif, Czech Republic. Int J Earth Sci 96: 623–638

Adams DM, Armstrong RS, Best SP (1981) Single-crystal Raman spectroscopic study of apophyllite, a layer silicate. Inorg Chem 20(6): 1771–1776

Apps JA (1983) Hydrothermal evolution of repository groundwaters in basalt. In: NRC Nuclear Waste Geo-

chemistry 83 US Nuclear Regulatory Commission Report NUREG/CP-0052, 14–51

Bucher K, Weisenberger TB (2013) Fluid-induced mineral composition adjustments during exhumation: the case of Alpine stilbite. Contrib Mineral Petrol 166(5): 1489–1503

Buriánek D, Novák M (2007) Compositional evolution and substitutions in disseminated and nodular tourmaline from leucocratic granites: examples from the Bohemian Massif, Czech Republic. Lithos 95(1–2): 148–164

Buriánek D, Dolníček Z, Novák M (2016) Textural and compositional evidence for a polyphaser saturation of tourmaline in granitic rocks from the Třebíč Pluton (Bohemian Massif). J Geosci 61(4): 309–334

Burkart E (1953) Mährens Minerale und ihre Literatur. Nakladatelství ČSAV, Praha. pp 1–1005 (in German)

Chipera SJ, Apps JA (2001) Geochemical stability of natural zeolites. In: Natural zeolites: occurrences, properties, applications. In: Bish DL, Ming DW (eds) Rev Mineral Geochem 45(1): 117–161

Coombs DS, Alberti A, Armbruster T, Artioli G, Colella C, Galli E, Grice JD, Libeau F, Minato H, Nickel EH, Passaglia E, Peacor DR, Quartieri S, Rinaldi R, Ross M, Sheppard RA, Tillmanns E, Vezzalini G (1997) Recommended nomenclature for zeolite minerals: report of the subcommittee on zeolites of the International Mineralogical Association, Commission on New Minerals and Mineral Names. Mineral Mag 62(4): 533–571

Černý P (1955) Minerals from amphibolite quarry in Mirošov (West Moravia). Čas Morav Mus 40: 93–107 (in Czech)

Černý P (1960) Milarite and wellsite from Věžná. Práce Brněn Zákl Čs Akad Věd 32: 1–16 (in Czech)

Černý P (1965a) Mineralogy of two pegmatites from the Věžná serpentinite. CSc thesis, Geological Institute of the ČSAV Prague, Prague, Czechoslovakia. pp 1–176 (in Czech)

Černý P (1965b) Thomsonite from Věžná in western Moravia. Čas Mineral Geol 10: 143–146 (in Czech)

Černý P, Povondra P (1965) Harmotome from desilicated pegmatites at Hrubšice, Western Moravia. Acta Univ Carol Geol 1: 31–43

Černý P, Smith JV, Mason RA, Delaney JS (1984) Geochemistry and petrology of feldspar crystallization in the Věžná pegmatite. Canad Mineral 22: 631–651

Černý P, London D, Novák M (2012) Granitic pegmatites as reflection of their sources. Elements 8: 289–294

Čopjaková R, Prokop J, Novák M, Losos Z, Gadas P (2021) Hydrothermal alterations of tourmaline from pegmatitic rocks enclosed in serpentinites; multistage processes with distinct fluid sources. Lithos 380: 105823

Deer AW, Howie AR, Wise SW, Zussman J (2004) Rock-forming minerals. Framework Silicates: Silica Minerals, Feldspathoids and the Zeolites. The Geological Society, London. pp 1–982

Dempsey ED, Holdsworth RE, Imber J, Bistacchi A, Di Toro G (2014) A geological explanation for intraplate earthquake clustering complexity: The zeolite-bearing fault/fracture networks in the Adamello Massif (Southern Italian Alps). J Struct Geol 66: 58–74

Dill HG, Füssl M, Botz R (2007) Mineralogy and (economic) geology of zeolite-carbonate mineralization in basic igneous rocks of the Troodos Complex, Cyprus. N Jb Mineral, Abh 183(3): 251–268

Dosbaba M, Novák M (2012) Quartz replacement by "kerolite" in graphic quartz-feldspar intergrowths from the Věžná I pegmatite, Czech Republic; A complex desilicification process related to episyenitization. Canad Mineral 50: 1609–1622

Evans BW, Hattori K, Barronet A (2013) Serpentinites: What, Why and When. Elements 9: 99–106

Finger F, Roberts MP, Haunschmid B, Schermaier A, Steyrer HP (1997) Variscan granitoids of central Europe: their typology, potential sources and tectonothermal relations. Mineral Petrol 61: 67–96

Frey M, Robinson D (eds.) (2009) Low-grade metamorphism. John Wiley & Sons. pp 1–351

Gadas P, Novák M, Staněk J, Filip J, Vašinová Galiová M (2012) Compositional evolution of zoned tourmaline crystals from pockets in common pegmatites, the Moldanubian Zone, Czech Republic. Canad Mineral 50: 895–912

Gadas P, Novák M, Szuszkiewicz A, Szełęg E, Galiová MV, Haifler J (2016) Manganoan Na, Be, Li-rich sekaninaite from miarolitic pegmatite at Zimnik, Strzegom-Sobótka Massif, Sudetes, Poland. Canad Mineral 54: 971–987

Gadas P, Novák M, Galiová MV, Szuszkiewicz A, Pieczka A, Haifler J, Cempírek J (2020) Secondary beryl in cordierite/sekaninaite pseudomorphs from granitic pegmatites – a monitor of elevated content of beryllium in the precursor. Canad Mineral 58: 785–802

Goryainov SV, Smirnov MB (2001) Raman spectra and lattice-dynamical calculations of natrolite. Eur J Mineral 13(3): 507–519

Green DI, Tindle AG, Moreton S (2005) Brewsterite-Ba and harmotome from the Wicklow lead mines, Co. Wicklow, Ireland. Irish J Earth Sci: 101–106

Guy A, Edel J, Schulmann K, Tomek Č, Lexa, O (2011) A geophysical Model of the Variscan orogenic root (Bohemian Massif): Implications for Modern Collisional Orogens. Lithos 124: 144–157

Hay RL, Sheppard RA (2001) Occurrence of zeolites in sedimentary rocks: An overview. Rev Mineral Geochem 45(1): 217–234

Iijima A (2001) Zeolites in petroleum and natural gas reservoirs. Rev Mineral Geochem 45(1): 347–402

James EW, Silver LT (1988) Implications of zeolites and their zonation in the Cajon Pass deep drillhole. Geoph Res Letters 15(9): 973–976

Janoušek V, Hanžl P, Svojtka M, Hora J, Kochergina Y, Gadas P, Holub FV, Gerdes A, Verner K, Hrdličková K, Daly S, Buriánek D (2020) Ultrapotassic magmatism at the hay day of the Variscan Orogeny – the story of the Třebíč Pluton, the largest durbachitic body in the Bohemian Massif. Int J Earth Sci 09: 1767–1810

Jiang S-Y, Yang JH, Novák M, Selway JB (2003) Chemical and boron isotopic compositions of tourmaline from the Lavičky leucogranite, Czech Republic. Geochem J 37: 545–556

Karlsson HR (2001) Isotope geochemistry of zeolites. Rev Mineral Geochem 45(1): 163–205

Kotková J (2007) High-pressure granulites of the Bohemian Massif: recent advances and open questions. J Geosc 52: 45–71

Kruťa T (1966) Moravian minerals and their literature 1940–1965. Moravské museum Brno. pp 1–879 (in Czech)

Kříbek B, Hájek A (eds) (2005) Uranium deposit Rožná: model of Late Variscan and after -Variscan mineralisations. Czech Geol. Survey, Prague, 89 pp, (in Czech)

Kříbek B, Žák K, Dobeš P, Leichmann J, Pudilová M, René M, Scharm B, Scharmová M, Hájek A, Holeczy D, Hein UF, Lehmann B (2009) The Rožná uranium deposit (Bohemian Massif, Czech Republic): shear zone-hosted, late Variscan and post-Variscan hydrothermal mineralization. Mineral Dep 44(1): 99–128

Lafuente B, Downs R T, Yang H, Stone N (2015) The power of databases: the RRUFF project. In: Armbruster T, Danisi RM (eds) Highlights in Mineralogical Crystallography. Berlin, Germany, W. De Gruyter, pp 1–30

Langella A, Cappelletti P, Gennaro RD (2001) Zeolites in closed hydrologic systems. Rev Mineral Geochem 45(1): 235–260

Larsen AO, Nordrum FS, Döbelin N, Armbruster T, Petersen OV, Erambert M (2005) Heulandite-Ba, a new zeolite species from Norway. Eur J Mineral 17(1): 143–153

Leeman WP, Sisson VB (1996) Geochemistry of boron and its implications for crustal and mantle processes. Rev Mineral 33: 645–707

Leichmann J, Gnojek I, Novák M, Sedlák J, Houzar S (2017) Durbachites from the Eastern Moldanubicum (Bohemian Massif): erosional relics of large, flat tabular intrusions of ultrapotassic melts–geophysical and petrological record. Int J Earth Sci 106: 59–77

Liou JG, Kim HS, Maruyama S (1983) Prehnite–epidote equilibria and their petrologic applications. J Petrol 24(4): 321–342

Liou JG, Maruyama S, Cho M (1985) Phase equilibria and mineral parageneses of metabasites in low-grade metamorphism. Mineral Mag 49: 321–333

Litochleb J, Černý P, Lantora M, Šrein V, Sejkora J (2000) The underground gas reservoir at Háje near Příbram (Central Bohemia) – knowlegde from mineralogical reserach. Bull mineral petrolog Odd Nár Muz (Praha) 8: 68–74 (In Czech)

Łodziński M, Wrzalik R, Sitarz M (2005) Micro-Raman spectroscopy studies of some accessory minerals from pegmatites of the Sowie Mts and Strzegom-Sobótka massif, Lower Silesia, Poland. J Mol Struct 744: 1017–1026

London D (2008) Pegmatites. Canad Mineral, Special Publication 10: pp 1–347

London D (2018) Ore-forming processes within granitic pegmatites. Ore Geol Rev 101: 349–383

London D, Morgan GB, Icenhower J (1998) Stability and solubility of pollucite in the granite system at 200 MPa H_2O. Canad Mineral 36(2): 497–510

London D, Morgan GB, Paul KA, Guttery BM (2012) Internal evolution of miarolitic granitic pegmatites at the Little Three mine, Ramona, California, USA. Canad Mineral 50(4): 1025–1054

Matte P, Maluski H, Rajlich P Franke, W (1990) Terrane boundaries in the Bohemian Massif: Result of large-scale Variscan shearing. Tectonophys 177: 151–170

Melleton J, Gloaguen E, Frei D, Novák M, Breiter K (2012) How are the time of emplacement of rare-element pegmatites, regional metamorphism and magmatism interrelated in the Moldanubian Domain of Variscan Bohemian Massif, Czech Republic. Canad Mineral 50: 1751–1773

Merlet C (1994) An accurate computer correction program for quantitative electron probe microanalysis. Mikrochim Acta 114: 363–376

Ming DW, Boettinger JL (2001) Zeolites in soil environments. Rev Mineral Geochem 45(1): 323–345

Moles N, Nawaz R (1996) Harmotome associated with Tertiary dyke intrusion in mineralised breccia at Newtownards, Northern Ireland. Irish J Earth Sci: 145–153

Mullis J, Dubessy J, Poty B, O'Neil J (1994) Fluid regimes during late stages of a continental collision: physical, chemical and stable isotope measurements of fluid inclusions in fissure quartz from a geotraverse through the Central Alps, Switzerland. Geochim Cosmochim Acta 58: 2239–2267

Neuhoff PS, Hovis GL, Balassone G, Stebbins JF (2004) Thermodynamic properties of analcime solid solutions. Amer J Sci 304(1): 21–66

Novák F, Pauliš P, Šikola D (2001) Witherite, harmotome and baryte from Rožná U-deposit. Bull mineral petrolog Odd Nár Muz (Praha) 9: 307–310 (in Czech)

Novák M, Černý P, Kimbrough DL, Taylor MC, Ercit TS (1998) U-Pb ages of monazite from granitic pegmatites in the Moldanubian Zone and their geological implications. Acta Univ Carol Geol 42: 309–310

Novák M, Kadlec T, Gadas P (2013) Geological position, mineral assemblages and contamination of granitic peg-

matites in the Moldanubian Zone, Czech Republic; examples from the Vlastějovice region. J Geosci 58: 21–47

Novák M, Gadas P, Cempírek J, Škoda R, Breiter K, Kadlec T, Loun J, Toman J, (2015a) B1 Granitic pegmatites of the Moldanubian Zone, Czech Republic. In PEG 2015: 7th International Sympopsium on Granitic Pegmatites, Field trip guidebook, 23–72

Novák M, Čopjaková R, Dosbaba M, Galiová MV, Všianský D, Staněk J (2015b) Two paragenetic types of cookeite from the Dolní Bory-Hatě pegmatites, Moldanubian Zone, Czech Republic: Proximal and distal alteration products of Li-bearing sekaninaite. Canad Mineral 53(6): 1035–1048

Novák M, Prokop J, Losos Z, Macek I (2017) Tourmaline, an indicator of external Mg-contamination of granitic pegmatites from host serpentinite; examples from the Moldanubian Zone, Czech Republic. Mineral Petrol 111: 625–641

Novotný F, Novák M, Cempírek J (2019) Chemical composition of tourmaline from the Dolní Rožínka elbaite pegmatite. Bull Mineral Petrolog 27 (1): 38–45 (in Czech with English abstract)

Palandri JL, Reed M (2004) Geochemical models of metasomatism in ultramafic systems: Serpentinization, rodingitization, and sea floor carbonate chimney precipitation. Geochim Cosmochim Acta 68: 1115–1133

Palinkaš SS, Wegner R, Čobić A, Palinkaš LA, Barreto SDB, Váczi T, Bermanec V (2014) The role of magmatic and hydrothermal processes in the evolution of Be-bearing pegmatites: Evidence from beryl and its breakdown products. Amer Miner 99(2-3): 424–432

Passaglia E (1970) The crystal chemistry of chabazites. Amer Miner 55(7-8): 1278–1301

Pauliš P, Cempírek J (1998) Harmotome and chabazite from desilicated pegmatite in Věžná near Bystřice nad Pernštejnem. Vlastivěd Sbor Vysočiny, Odd Všd přír 13: 349–350 (in Czech)

Pauliš P, Šikola D (1999) Pyrite-zeolite mineral assemblage at U-deposit Rožná. Minerál 7: 310–314 (in Czech)

Pauliš P, Sejkora J, Novák F, Malíková R (2014) Harmotome and stilbite-Ca from the base-metal deposit Křižanovice in Železné hory Mountains (Czech Republic). Bull mineral petrolog Odd Nár Muz (Praha) 22(1): 68–73 (in Czech)

Perrotta AJ (1976) A low-temperature synthesis of a harmotome-type zeolite. Amer Miner 61(5-6): 495–496

Pertoldová J, Týcová P, Verner K, Košuličová M, Pertold Z, Košler J, Konopásek J, Pudilová M (2009) Metamorphic history of skarns, origin of their protolith and implications for genetic interpretation; an example from three units of the Bohemian Massif. J Geosci 54(2): 101–134

Pertoldová J, Verner K, Vrána S, Buriánek D, Štědrá V, Vondrovic L (2010) Comparison of lithology and tectonometamorphic evolution of units at the northern margin of the Moldanubian Zone: implications for geodynamic evolution in the northeastern part of the Bohemian Massif. J Geosc 55(4): 299–319

Pieczka A, Szuszkiewicz A, Szeleg E, Janeczek J, Nejbert K (2015) C1 Granitic pegmatites of the Polish part of the Sudetes. In PEG 2015: 7th International Sympopsium on Granitic Pegmatites, Field trip guidebook: 73–103

Řídkošil T, Knížek F (1987) Zeolite mineralization and occurrence of whewellite at Příbram U-deposit. Sbor Semin "Mineralogia uranových a s nimi súvisiacich nerastných surovín", Uránový priezkum Spišská Nová Ves, 126–130 (In Czech)

Sahama TG, Lehtinen M (1967) Harmotome from Korsnäs, Finland. Mineral Mag 36(279): 444–448

Schilling J, Marks MAW, Wenzel T, Vennemann T, Horváth L, Tarassoff P, Jacob DE, Markl G (2011) The magmatic to hydrothermal evolution of the intrusive Mont Saint-Hilaire Complex: insights into the late-stage evolution of peralkaline rocks. J Petrol 52: 2147–2185

Schulmann K, Lexa O, Janoušek V, Lardeaux JM, Edel JB (2014) Anatomy of a diffuse cryptic suture zone: An example from the Bohemian Massif, European Variscides. Geology 42(4): 275–278

Spürgin S, Weisenberger TB, Marković M (2019) Zeolite-group minerals in phonolite-hosted deposits of the Kaiserstuhl Volcanic Complex, Germany. Amer Miner: J Earth Planet Materials 104(5): 659–670

Stefansson A, Gíslason SR (2001) Chemical weathering of basalts, southwest Iceland: effect of rock crystallinity and secondary minerals on chemical fluxes to the ocean. Amer J Sci 301: 513–556

Šťáva F (1981) Discovery of zeolite minerals in west Moravia (Eastern Moldanubicum). Čas Mineral Geol 26: 433 (in Czech)

Tajčmanová L, Konopásek J, Schulmann K (2006) Thermal evolution of the orogenic lower crust during exhumation within a thickened Moldanubian root of the Variscan belt of Central Europe. J Metam Geol 24(2): 119–134

Teertstra DK, Černý P (1995) First natural occurrences of end-member pollucite: A product of low-temperature reequilibration. Eur J Mineral 7**:** 1137–1148

Teertstra DK, Černý P (1997) The compositional evolution of pollucite from African granitic pegmatites. J African Earth Sci 25: 317–331

Teertstra DK, Lahti SI, Alviola R, Černý P (1993) Pollucite and its alteration in Finnish pegmatites. Geol Sur Finland Bull 368, Geologian tutkimuskeskus, pp 1–39.

Teertstra DK, Černý P, Novák M (1995) Compositional and textural evolution of pollucite in rare-element pegmatites of the Moldanubicum. Mineral Petrol 55: 37–52

Teertstra DK, Černý P, Langhof J, Smeds SA, Grensman F (1996) Pollucite in Sweden: Occurrences, crystal

chemistry, petrology and subsolidus history. GFF 118: 141–149

Toman J, Novák M, (2018) Textural relations and chemical composition of minerals from a pollucite + harmotome + chabazite nodule in the Věžná I pegmatite, Czech Republic. Canad Mineral 56(4): 375–392

Toman J., Novák M. (2020) Beryl-columbite pegmatite Věžná I. Acta Mus Morav, Sci Geol 105(1): 3–42 (in Czech)

Tschernich RW (1992) Zeolites of the World. Geoscience Press Phoenix., pp 1–563

Uhlík Z, Řídkošil T (1987) Relation of zeolite mineralization and ores at the U-deposit Rožná. Sbor Semin "Mineralogia uranových a s nimi súvisiacich nerastných surovín", Uránový priezkum Spišská Nová Ves: 107–110 (in Czech)

Utada M (2001a) Zeolites in burial diagenesis and low-grade metamorphic rocks. In: Bish DL, Ming DW (eds) Natural zeolites: occurrences, properties, applications. Rev Mineral Geochem 45(1): 277–304

Utada M (2001b) Zeolites in hydrothermally altered rocks. Rev Mineral Geochem 45(1): 305–322

Vávra V (1997) Mineral assemblages from Alpine-type veins at Mirošov (near Nové Město na Moravě. Acta Mus Morav, Sci Nat 81: 25–39 (in Czech)

Verner K, Buriánek D, Vrána S, Vondrovic L, Pertoldová J, Hanžl P, Nahodilová R (2009) Tectonometamorphic features of geological units along the northern periphery of the Moldanubian Zone. J Geosci 54(2): 87–100

Warr LN (2021) IMA-CNMNC approved mineral symbols. Mineral Mag 85(3): 291–320

Weisenberger T (2009) Zeolites in fissures of crystalline basement rocks. Unpublished Ph.D. thesis, Universität Freiburg, Freiburg, Germany. pp 1–161

Weisenberger T, Bucher K (2010) Zeolites in fissures of granites and gneisses of the Central Alps. J Metam Geol 28(8): 825–847

Weisenberger T, Bucher K (2011) Mass transfer and porosity evolution during low temperature water–rock interaction in gneisses of the Simano nappe: Arvigo, Val Calanca, Swiss Alps. Contr Mineral Petrol 162(1): 61–81

Weisenberger T, Selbekk RS (2009) Multi-stage zeolite facies mineralization in the Hvalfjördur area, Iceland. Int J Earth Sci 98: 985–999

Weisenberger TB, Spürgin S, Lahaye Y (2014) Hydrothermal alteration and zeolitization of the Fohberg phonolite, Kaiserstuhl Volcanic Complex, Germany. Int J Earth Sci 103(8): 2273–2300

Williams ML, Carr PF (2005) Isotope systematics of secondary minerals from the Prospect Intrusion, New South Wales. Aust J Earth Sci 52(6): 799–806

Zhang Q, Qin F, Niu JJ, Wu X (2018) High-pressure investigation on prehnite: X-ray diffraction and Raman spectroscopy. High Temperatures-High Pressures 47(3): 213–221